Title:

FRG1 Regulates Nonsense-Mediated mRNA Decay by Modulating UPF1 Levels

Authors:

Ananya Palo[1,2], Talina Mohapatra[1,2], Anamika Singh[1,2], Shithij Thalakkat[1,2], Suryasikha Mohanty[3], Rajeeb Kumar Swain[3] , Manjusha Dixit[1,2] *

Affiliations:

[1] National Institute of Science Education and Research, School of Biological Sciences, Bhubaneswar, Odisha 752050, India

[2] Homi Bhabha National Institute, Training School Complex, Anushakti Nagar, Mumbai 400094, India

[3] Institute of Life Sciences, Nalco Square, Chandrasekharpur, Bhubaneswar, Odisha 751023, India

***Corresponding author:**

Manjusha Dixit, PhD

Associate Professor

Room No. 204, School of Biological Sciences,

National Institute of Science Education and Research, Bhubaneswar

PO: Jatani, Khurda 752050, Odisha, India

Phone: Office 91-674 2494195, Lab 91-674-2494196

Email ID: manjusha@niser.ac.in

ORCID IDs

Ananya Palo	0000-0001-5276-2742
Anamika Singh	0009-0006-8423-6898
Shithij Thalakkat	0009-0008-3127-9979
Suryasikha Mohanty	0009-0003-6957-3245
Rajeeb Kumar Swain	0000-0003-4815-8221
Talina Mohapatra	0000-0002-0902-360X
Manjusha Dixit	0000-0002-6997-1054

Abstract:

FRG1 acts as a molecular double-edged sword: while its overexpression is linked to facioscapulohumeral muscular dystrophy (FSHD), it's under expression activates tumorigenic signalling pathways—highlighting the importance of tightly regulated FRG1 levels. Although prior studies have hinted at FRG1's involvement in RNA biogenesis, its core molecular functions have remained largely elusive. Our previous work identified FRG1 as a transcriptional regulator of genes in the nonsense-mediated decay (NMD) pathway; however, the underlying mechanisms were not fully delineated.

In this study, using a range of cellular models with altered FRG1 expression, we demonstrate that reduced FRG1 levels enhance NMD activity. We reveal that FRG1 is a structural component of both the spliceosome and the exon junction complex (EJC), and that it directly modulates NMD by interacting with UPF1—regulating its ubiquitination and degradation. Furthermore, we show that DUX4 inversely regulates the NMD machinery through FRG1, establishing a critical molecular axis. Despite its structural association with the EJC and spliceosome, the absence of FRG1 does not compromise the integrity of these complexes. Polysome profiling showed that FRG1 co-sediments with eIF4A3, a core EJC component, across translating ribosomal fractions. This interaction was further supported by proximity ligation assays confirming the close spatial proximity of FRG1 and eIF4A3. Importantly, we validated the impact of FRG1 perturbation on NMD efficiency and UPF1 levels in vivo using a transgenic FRG1 knockout zebrafish model.

Together, these findings establish a direct, DUX4-independent role for FRG1 in regulating the NMD pathway and uncover a previously unrecognized function for FRG1 in post-transcriptional gene regulation. Our work provides mechanistic insight into FRG1's molecular

53 roles and lays the groundwork for therapeutic strategies targeting diseases associated with its
54 dysregulation.

55

56 **Key Words:** FSHD region gene 1, NMD, DUX4, UPF1, Structural component, Proteasomal
57 degradation

58

59 **Introduction:**

60 In eukaryotic organisms, gene expression undergoes quality control at various stages.
61 One pivotal mechanism of RNA quality control is the Nonsense-mediated mRNA decay
62 (NMD) pathway. NMD plays a critical role in preserving cellular equilibrium by degrading
63 messenger RNAs (mRNAs) containing premature termination codons (PTCs), thus preventing
64 the synthesis of potentially harmful proteins. Interest in NMD has been further fuelled by the
65 studies showing the regulation of half-life and, thereby steady-state abundance of nearly 5-10%
66 of mammalian transcriptome having upstream open reading frame (uORFs) in the 5'UTR,
67 presence of long 3'UTR or 3'UTR harboring an intron, presence of uORF that interferes with
68 the expression of main ORF, and downstream EJCs [1,2]. NMD is known to regulate various
69 biological processes, including development, stress response, cell differentiation, and cell
70 proliferation [3–9]. The loss of key NMD factors-UPF1, UPF2, or SMG1-results in embryonic
71 lethality in mice, highlighting their essential role [10–12]. Evidence also suggests differential
72 NMD activity across cell and tissue types. For instance, analysis of NMD reporters and various
73 NMD substrates demonstrated higher NMD efficiency in HeLa cells compared to MCF7 cells
74 [13]. Furthermore, RNAi-mediated depletion of NMD factors such as UPF1 or SMG1 led to

DNA damage and inhibited the growth of HeLa cells, but not fibroblasts [14]. Together, these findings indicate that NMD is a highly regulated and context-dependent process.

The importance of NMD pathway has been highlighted as numerous genetic diseases that result from misexpression of faulty mRNAs escaping the mRNA surveillance pathway. Mutations in NMD factor UPF3B result in neurodevelopmental disorder, ADHD, autism, and schizophrenia [15–17]. Dysregulation of NMD factors like UPF2, UPF3A, SMG6, eIF4A3, RNPS1 results in intellectual disability (ID) disorder [18,19]. Aberrant NMD is associated with cancer [20,21]. For example, mutations in UPF1 lead to inflammatory myofibroblastic tumors (IMT) and pancreatic cancer [22,23]. Deletion of one allele of SMG1 results in lung cancer and hematopoietic malignancies [24]. Upregulation of AKT results in increased cancer cell proliferation [25–27]. Additionally, tumors may benefit from NMD-mediated degradation by acquiring PTCs in tumor suppressor genes like WT1, TP53, RB, and BRCA1/2 [28–30].

This dual role of NMD in degrading aberrant mRNAs and post transcriptionally targeting a subset of normal mRNAs is believed to occur through different pathways. Gehring et al. identified two branches of NMD - UPF2 and RNPS1 or EJC dependent [31]. Subsequently, Chen et al. identified a branch of NMD pathway that is independent of UPF3B [32]. Ultimately, the SURF complex assembles on the aberrant transcripts which are degraded via the DECID complex [33–36]. Despite significant progress in understanding the NMD pathway, critical gaps remain, particularly in deciphering the precise molecular mechanisms that govern its specificity and efficacy. The emerging evidence of a broader role for NMD in gene expression regulation raises pressing questions: How is the NMD response buffered? How are transcripts without PTCs selectively targeted by the NMD machinery? And, importantly, is the NMD pathway itself subject to regulatory control? Addressing these gaps is essential for a comprehensive understanding of NMD's role in cellular processes and disease. In the past,

with an intent to discover novel NMD genes that may aid in therapeutic interventions for genetic diseases, primary genetic screens were conducted in model organisms that resulted in identification of factors such as ROD1, ICE1, DHX34, NBAS [37–39]. Immunoprecipitation to identify the interacting proteins of NMD factor ROD1 (EJC component) unveiled the binding of FRG1 with the former [37], hinting towards a direct or indirect role played by FRG1 (FSHD Region Gene 1) in NMD.

FRG1 is a gene with increased expression leading to facioscapulohumeral muscular dystrophy (FSHD) [40–42] while reduced expression is linked to several types of cancer including oral, gastric, colorectal, prostrate, and breast cancer [43–46]. Some reports suggest potential role of FRG1 in RNA biogenesis. FRG1 has been found to localise within the nucleolus in HeLa cells and associates with Cajal bodies, nucleoli and nascent transcripts in *Xenopus laevis* oocytes [47]. RIP-based assay in HeLa and C2C12 cells shows the direct binding of FRG1 with FXR1 and Rbfox1 mRNA, respectively [47,48]. Yeast two hybrid assays have shown FRG1 to be a part of spliceosome B_{act}/ C complex [49]. In the same study, co-immunoprecipitation revealed binding of CWC22 with FRG1 and eIF4A3. CWC22 is an essential splicing factor that initiates EJC assembly via direct interaction with EJC core protein eIF4A3 [50]. Cryo EM structure by Bertram et al. showed intricate spatial organisation of FRG1 within spliceosome C complex. Here, FRG1 was shown to interact with NTD (N-terminal domain) of splicing factor PRP8 [51]. The aforementioned studies showing FRG1's interaction with spliceosome and EJC gave a plausible hint of its role in the post transcriptional processing of transcripts. Additionally, our previous work revealed that FRG1 depletion affects transcript level of NMD factors (ICE1, PNN, MAGOH, ROD1, UPF3B, SMG1) having roles in different steps of the NMD pathway [52]. However, whether FRG1 affects NMD, and if so, whether FRG1 acts as a structural component of the NMD machinery, remains unclear, as does the exact mechanism by which FRG1 regulates the NMD pathway within the cell.

124 In this manuscript, we have employed NMD loss-of-function and gain-of-signal luciferase
125 reporter systems, as well as an intron-retention splicing construct, to investigate the impact of
126 altered FRG1 expression on nonsense-mediated mRNA decay (NMD) activity. We have
127 utilized both FRG1 knockout and overexpression cellular models to systematically examine its
128 role in modulating NMD efficiency. Additionally, we have performed transcriptome analyses
129 to assess changes in the expression of known NMD target transcripts, particularly those
130 harboring premature termination codons (PTCs). To probe the structural and functional
131 associations of FRG1 within the spliceosome–EJC–NMD machinery, we conducted co-
132 immunoprecipitation, polysome profiling, and proximity ligation assays. Furthermore, we
133 evaluated the in vivo relevance of our in vitro experiments using a transgenic frg1 knockout
134 zebrafish model. Our findings offer new insights confirming FRG1's role in modulating the
135 NMD pathway, and its underlying molecular mechanism.

136

137 **Materials and Methods:**

138 **Zebrafish maintenance:**

139 AB strain of zebrafish was used in this study. The animal work was approved by the
140 Institutional Animal Ethics Committee. Inclusion criteria were fertilized one-cell stage
141 embryos from healthy adult breeders (6–12 months; female:male ratio 2:1) with normal
142 morphology and survival beyond 24 hpf. Exclusion criteria included unfertilized eggs,
143 developmental arrest, abnormal morphology, or infection. Embryos were raised in E3 media
144 (34.8 gm NaCl, 1.6 gm KCl, 5.8 gm $CaCl_2.2H_2O$, 9.78 gm $MgCl_2.6\ H_2O$; pH-7.2) at 28°C. At
145 24 hpf, embryos were bleached using 0.001% sodium hypochlorite solution (Sigma Aldrich,
146 MO, USA) to prevent any kind of infection. These were then transferred into a circulating water
147 system tank (Techniplast, Odisha, India) at 5 dpf. Embryos were randomized by clutch, with

148 microinjections performed by one investigator and phenotyping assessed by blinded
149 evaluators.

150 **frg1 knockout generation:**

151 To generate frg1 knockout transgenic zebrafish line, sgRNAs targeting frg1 exon1 and exon 9
152 (sequences mentioned in Supplementary Table S1) were designed following the protocol by
153 Varsheney et al. [53]. The gene-specific oligos were annealed with the 5'-
154 AAAAGCACCGACTCGGTGCCACTTTTTCAAGTTGATAACGGACTAGCCTTATTTT
155 AACTTGCTATTTCTAGCTCTAAAAC-3' (gRNA backbone) using Phusion polymerase
156 (Thermo Scientific, IL, USA). The guide RNAs were in vitro transcribed using MEGAscript™
157 SP6 Transcription Kit (Invitrogen) and Megascript™ T7 transcription kit (Invitrogen, MA,
158 USA), respectively. Cas9 mRNA was synthesized by linearizing the pCs2-nCas9n nanos 3'
159 UTR vector (Addgene, #62542) with XbaI-HF (NEB, MA, USA) followed by in vitro
160 transcription using mMESSAGE mMACHINE™ transcription kit (Invitrogen). The adult male
161 and female fishes were bred, and eggs were collected at 1-celled stage. A Femtojet
162 microinjector (Eppendorf, Hamburg, Germany) was used to inject embryos with a mixture
163 containing 25 ng/µl each of exon1 and exon 9 sgRNAs, along with 100 ng/µl Cas9 mRNA.

164 **Screening of frg1 knockout zebrafish embryos**:

165 Embryos were genotyped three months post-injection to screen for mutation incorporation,
166 using caudal fin clipping across F0, F1, and F2 generations. Genomic DNA was isolated using
167 1x TE buffer (10 mM Tris-HCl, pH 7.5, and 1 mM EDTA, pH 8.0) along with proteinase K
168 treatment (Roche, Basel, Switzerland), followed by PCR using exon-1 forward and exon-9
169 reverse primers with primers listed in Supplementary Table S1.

170 **Whole mount in-situ hybridisation (WISH):**

171 WISH was performed on zebrafish embryos as described earlier (Thisse and Thisse, 2008) [54].
172 Briefly, the zebrafish frg1 coding sequence (Supplementary Table S1) was amplified and
173 cloned in pCR™-Blunt II-TOPO (Invitrogen). The DIG (Digoxigenin) labelled RNA probe
174 was synthesized by linearizing the plasmid with BamH1 (NEB) and transcribing with T7
175 polymerase. The embryos were then fixed, dehydrated through methanol series (25% to 100%)
176 and stored at -20°C in 100% methanol.–After rehydration, the embryos were incubated in a
177 hybridization buffer containing 50% deionized formamide, 5X SSC, 50 µg/ml heparin, 0.5
178 mg/ml torula RNA, 9.2 mM citric acid, and 0.1% Tween-20, along with a zebrafish FRG1-
179 specific probe. The following day, embryos were incubated in 2% blocking reagent (Roche-
180 1109617600) for 2 hours at room temperature, to prevent non-specific binding. Staining of
181 embryos was done by incubating them with anti-digoxigenin (Roche) FAB fragment coupled
182 with alkaline phosphate diluted in blocking buffer. On the 3rd day, embryos were washed with
183 MABT (Maleic Acid buffer with Tween) and pH9 buffer at room temperature and then
184 transferred into BM purple dye (Roche) for color development, in dark.

185 **Cell culture, Transfection and stable line generation:**

186 MCF7 cells were obtained from Cell Repository, NCCS, Pune, India. The cell line was
187 authenticated by the repository using 16 STR markers (AmpFISTR Identifier Plus PCR
188 Amplification Kit, Applied BioSystems). We checked mycoplasma contamination using
189 MycoAlert Mycoplasma Assay kit (Lonza). The cell line was grown in DMEM media
190 (Himedia, Mumbai, India) supplemented with 10% FBS (Himedia, US origin) and 1X
191 Penicillium-Streptomycin-Amphotericin B (PSA; Himedia, Mumbai, India). Cells were
192 cultured at 37°C and 5% CO_2. FRG1 knockdown (pLKO.1_FRG1sh, TRCN0000075012,
193 RRID: AB_259684) and expression (HsCD004 21091 PLX304_FRG1) vectors were procured
194 from Sigma and Harvard repository, respectively. Transfection of the cells was done with the
195 constructs using Lipofectamine 3000 according to the manufacturer's protocol (Invitrogen).

196 Single-cell colonies were selected for overexpression and knockdown using blasticidin (10
197 µg/ml) and puromycin (2 µg/ml) (Sigma Aldrich, MO, USA) antibiotics, respectively.
198 Confirmation of the stable lines was done using Western Blotting.

199 **NMD assay:**

200 NMD sensitive luciferase reporter (pCMV-3XFLAG-Fluc-betaglobin-39PTC) was purchased
201 from Addgene repository (Addgene:#112084). pKC-4.06 plasmid was a kind gift from Dr.
202 James Inglese's lab (pKC-4.06 plasmid was a kind gift from Dr. James Inglese's lab RRID:
203 Addgene_112084) [38]. The NMD sensor plasmid was microinjected into 1-cell stage
204 zebrafish embryos. It was also transfected in MCF7 perturbed cells
205 (MCF7_FRG1_overexpressed, MCF7_FRG1_Knockout and MCF7_FRG1_Knockdown) and
206 their corresponding control cells (MCF7_Empty Vector, MCF7_Wild type and
207 MCF7_Scrambled), respectively using Lipofectamine 3000 (Invitrogen, MA, USA) in a 12
208 well plate at 50% cell confluency. 48 h post transfection, cell lysate was prepared according to
209 manufacturer's protocol (Promega, WI, USA). Luciferase signal was recorded using
210 Varioskan® Flash Multimode Reader (Thermo Scientific, MA, USA). Experiment was
211 performed in triplicate.

212 **Co Immunoprecipitation:**

213 MCF7 cells (11 million) were plated and grown in 150 mm dishes. The cells were washed with
214 DPBS (Himedia) and fixed using 1% formaldehyde (Himedia) for 10 minutes at room
215 temperature. Reaction was stopped using 1.25M glycine solution (MP Biomedicals, OH, USA).
216 Cells were scrapped after adding ice-cold PBS and lysed using non-denaturing mammalian
217 lysis buffer (20 mM Tris, pH-7.5, 150 mM NaCl, 1 mM EDTA, 1 mM EGTA, 1% NP-40)
218 along with protease inhibitor (Invitrogen). Cell lysate was prepared by sonicating cells at 40%
219 amplitude, 30 sec OFF/ON cycle, 5 times using a Ultrasonic Processor Sonicator (Cole-Parmer,
220 IL, USA). The cell lysate was centrifuged at maximum speed for 10 mins at 4°C to collect the
221 supernatant. The supernatant was divided into three equal parts- whole cell lysate, IgG
222 (negative control), and test sample (antibody of interest). Immunoprecipitation was performed

223 overnight at 4°C by incubating the samples with 5 µg of respective primary antibodies [(FRG1,
224 Abcam, MA, USA), (GAPDH, Abgenex, India), (DUX4, Novus Biologicals, CO, USA),
225 (UPF1, CST, MA, USA), eIF4A3 (Abcam, MA, USA), CWC22 (Abcam, MA, USA), IgG
226 (H+L) (Rockland, USA), PRP8 (Abcam, MA, USA), UPF3B (Abcam, MA, USA)]. Following
227 day, protein A agarose bead (Santa Cruz Biotechnology, TX, USA) was washed with 1x PBS
228 and incubated with the samples at 4°C for 8 hours. Post incubation, beads were extensively
229 washed with ice cold PBS, boiled for 5 min with Laemlli buffer. Subsequently, immunoblotting
230 was carried out. The bands were detected by chemiluminescence using SuperSignal™ West
231 Femto maximum sensitivity substrate (Thermo Scientific). Band intensities were normalised
232 to GAPDH.

233 **Proteasome inhibition:**

234 In a 12-well plate, 0.1 million MCF7 cells having DUX4 overexpression were plated in three
235 wells. Post 12 hours, FRG1 expression vector (1 µg) was transfected in one of the wells using
236 Lipofectamine 3000 (Invitrogen). Induction with 500 ng/ml doxycycline (MP Biomedicals)
237 was done for a period of 24 hours. Post 16 hours of induction, MG132 (50 µM) (Sigma Aldrich,
238 MA, USA) was added in this condition (DUX4 induction along with FRG1 expression).
239 Subsequently, western blotting was carried out to visualise the proteasomal inhibition.

240 **Western Blotting:**

241 Whole cell protein lysate was prepared using ice-cold RIPA buffer (Thermo Scientific, IL
242 USA) and a cocktail of protease and phosphatase inhibitor (Thermo Scientific). BCA protein
243 assay kit (Thermo Scientific) was used to quantify the total protein concentration. 30 µg of
244 protein samples were loaded and resolved on 12% sodium dodecyl sulfate polyacrylamide gel
245 electrophoresis (SDS-PAGE) and transferred onto PVDF membrane (Millipore, Bangalore,
246 India). Membrane blocking was done using 5% skimmed milk (MP Biomedicals) for an hour

247 and incubated overnight with respective antibodies of interest. Next day, blot washing was
248 done using 1x TBST buffer and incubated with HRP conjugated secondary antibody for one
249 hour. Blots were again washed with 1x TBST buffer and detected in Chemidoc using
250 SuperSignal™ West Femto maximum sensitivity substrate (Thermo Scientific). Images were
251 analysed in Image J software (NIH, MD, USA) RRID: SCR_003070. All experiments were
252 performed in triplicate.

253 **Quantitative Real Time PCR:**

254 Total RNA was isolated from MCF7 cells. frg1 transgenic knockout and AB strain wild type
255 zebrafish using RNeasy mini kit (Qiagen, Hilden, Germany). Reverse transcription was
256 performed using verso cDNA synthesis kit (Thermo Scientific, Lithuana) with 1µg of total
257 RNA according to manufacturer's instructions. Each RT-PCR reaction was carried out using
258 20ng cDNA, 2x SYBR Green PCR Master Mix (Thermo Scientific, CA, USA), and respective
259 primers (Supplementary Table S1) using QS-7 system (Applied Biosystem- Thermo Scientific,
260 CA, USA). The experiment was carried out in triplicate using GAPDH as an internal control
261 (cell lines) and EF1A (zebrafish). Fold change was calculated using $2^{-\Delta\Delta CT}$ method.

262 **Library preparation for RNA-seq:**

263 Total RNA was isolated from MCF7 FRG1 perturbed cell lines (knockout and knockdown)
264 following manufacturer's instructions as described above. RNA was quantified using
265 NanoDrop One^{c} 2000 (Thermo Scientific). Purity of the samples were assessed using 2100
266 Bioanalyzer (Agilent Technologies, Waldbronn, Germany). Samples with RNA Integrity
267 Number (RIN>8) were considered for library preparation. Sequencing libraries were prepared
268 using 1 µg of total RNA for each sample with the Illumina TruSeq Stranded Total RNA Library
269 Prep Human/Mouse/Rat Kit (Illumina, CA, USA). mRNA was isolated from these samples
270 using magnetic beads with mRNA isolation kit (Poly A mRNA isolation module, NEB). Next,

271 this mRNA was used to synthesize double-stranded cDNA using NEBNext Ultra II RNA
272 library Preparation kit, according to the manufacturer's instructions. Then indexing adapters
273 were ligated to each sample. To generate NGS libraries, the products were enriched using PCR
274 with adapter universal primers and purified using SPRIselect beads. The prepared libraries
275 were quantified and checked for fragment size using the Qubit High Sensitivity DNA Reagent
276 (Qubit 2.0) followed by TapeStation D1000 ScreenTape (Agilent Technologies). Sequencing
277 of the resulting NGS libraries were performed using the NextSeq550 platform (llumina).

278 **Transcript Quantification, Isoform ratio measurements, and PTC prediction:**

279 The quality of the RNA-Seq data was assessed using FastQC (v0.12.2, RRID: SCR_014583))
280 to ensure high-quality sequencing reads. Transcript quantification was performed using
281 Salmon (version 1.7.0) for all the samples by using the Salmon generated *decoy-aware*
282 transcriptome index prepared using the Gencode SCR_014966 reference files (Release 47;
283 GRCh38/hg38) reference files. The command included parameters specifying the library type:
284 ISF, enabling validation of mappings, and correcting for sequence-specific biases [55]. The
285 expressed isoform from each gene, as determined by the transcripts per million (TPM) from
286 Salmon, was used for downstream analyses.

287 To investigate isoform usage and identify transcripts containing PTCs, quantified RNA-Seq
288 data were analyzed using IsoformSwitchAnalyzeR (version 2.2.0), an R package [56]. Isoforms
289 were categorized based on annotations from GENCODE release 47. IsoformSwitchAnalyzeR
290 identifies NMD-sensitive transcripts using the 50-nucleotides rule [57–60].

291 Significant isoform switches were determined by applying thresholds on the differential
292 isoform fraction ($|dIF| > 0.1$) and FDR corrected P-value (q-value; $q < 0.05$). Q-values were
293 computed using the DEXSeq-based statistical framework implemented in
294 IsoformSwitchAnalyzeR [61,62]. To facilitate visualization, illustrating isoform usage changes
295 between conditions, density plots were generated using the ggplot2 (version 3.5.1, RRID-

296 SCR_014601) package in R. Data set overlaps were analyzed using the ComplexHeatmap
297 (version 2.18.0) package of R and visualized as an UpSet plot [63]. All scripts for the RNA-
298 Seq analysis and NMD-prediction are available at GitHub https://github.com/sugar-
299 syrup/FRG1-NMD.

300 **Polysome Assay**

301 MCF7 cells were maintained in complete medium at 37 °C and treated with 100 μg/mL
302 cycloheximide for 30 min to stabilize polysomes. Cells were washed with ice-cold PBS
303 containing cycloheximide, lysed in hypotonic buffer (200 mM Tris-HCl [pH 7.4], 100 mM
304 KCl, 5 mM $MgCl_2$, 1% Nonidet P-40, 5 mM DTT, 40 U/mL RNasin, and protease inhibitors),
305 and layered onto 10–40% sucrose gradients (50 mM Tris-HCl [pH 7.4], 5 mM $MgCl_2$, 100 mM
306 KCl). Lysates were ultracentrifuged at 36,000 rpm for 2 h at 4 °C using Beckman SW41 rotor.
307 Gradients were fractionated using a fractionator (Biocomp gradient station and fraction
308 collector) with continuous monitoring at 254 nm. Proteins from each fraction were ethanol-
309 precipitated, resuspended in SDS sample buffer, resolved by 12% SDS-PAGE, and analyzed
310 via immunoblotting.

311 **Proximity Ligation Assay**

312 To assess protein–protein interactions, MCF7 cells were fixed in 4% paraformaldehyde and
313 permeabilized with 0.2% Triton X-100. (RRID:CVCL_0031) Following permeabilization,
314 cells were blocked using 2% bovine serum albumin (BSA) in PBS to reduce nonspecific
315 binding. Cells were then incubated with primary antibodies targeting FRG1 (mouse
316 monoclonal, Abnova, Taiwan) and eIF4A3 (rabbit monoclonal, Abcam, USA), raised in
317 different host species to enable dual recognition. The proximity ligation assay was performed
318 using the Duolink® In Situ PLA Red Kit (Cat. No. DUO92101, Sigma-Aldrich) according to
319 the manufacturer's instructions. Species-specific PLA probes (PLUS and MINUS) were
320 applied, and if the target proteins were in close proximity (<40 nm), the probes ligated to form

321 a circular DNA molecule. This DNA was subsequently amplified by rolling circle amplification
322 and visualized as distinct red fluorescent puncta under a fluorescence microscope. The number
323 of dots indicates the level of protein–protein interaction. As a negative control, parallel samples
324 were processed without the addition of primary antibodies. These control samples underwent
325 the same procedure with PLA probes and amplification reagents to assess background signal
326 due to nonspecific probe interaction or amplification.
327 See Supplementary Tables for detailed information on sources of reagents, software, and
328 antibodies.

329 **Results:**

330 **FRG1 expression perturbation alters NMD efficacy**

331 Based on our previous publication showing FRG1 as a direct transcriptional activator
332 of NMD genes [52], we assessed the effect of its expression levels on NMD efficacy. To
333 achieve this, we transiently transfected a specialized NMD sensor (pKC-4.06) in MCF7 cells
334 having knockdown, knockout, and ectopic expression of FRG1. An increase in luciferase
335 activity suggests impaired NMD machinery if PTCs are retained within transcripts in NMD
336 sensor, and vice versa. As shown in Fig. 1 A-B, depletion and knockout of FRG1 resulted in
337 decreased luciferase signal (0.8 and 0.83-folds, respectively) from the NMD sensor, indicating
338 an increase in NMD efficiency. Ectopic expression of FRG1 resulted in increased luciferase
339 signal (3.63-fold) from the NMD sensor, indicating reduced NMD efficiency (Fig. 1 C). To
340 validate our *in vitro* observation, evaluating FRG1 expression perturbation on NMD efficacy,
341 we generated FRG1 knockout zebrafish model. For this, we used CRISPR-Cas9 method,
342 injecting sgRNAs targeting exon-1 and 3'UTR regions of frg1 in AB strain zebrafish (Fig. 1
343 D-G). This was designed to delete most of the entire frg1 locus in zebrafish. The knockout of
344 frg1 in zebrafish was validated using PCR and Whole-mount in situ hybridization (Suppl. Fig.

345 1). To carry out NMD assay, 1- cell stage embryos were collected and microinjected with NMD
346 sensor construct. Reporter activity between knockout and control zebrafish embryos showed
347 enhanced NMD efficiency 48hour post fertilization (lane-2) (Fig. 1 H). Microinjecting the
348 NMD sensor construct along with FRG1 overexpression plasmid in the frg1$^{-/-}$ zebrafish
349 embryos at 1-cell stage resulted in reduced NMD efficacy as observed at 48 hours post-
350 fertilization (lane-3) (Fig. 1 H). These findings suggest that NMD is affected by FRG1.

351 **FRG1 depletion regulates abundance of PTC-containing transcripts**

352 Genome-wide RNA sequencing analysis was performed on FRG1 knockout,
353 knockdown, and their respective control cells to assess whether increased NMD efficiency
354 upon FRG1 depletion results in a decreased abundance of RNA isoforms containing premature
355 translation termination codons. Fig. 1 I, J shows that the knockdown of FRG1 led to a reduced
356 abundance of transcript isoforms containing PTCs. Among the top 10 genes having altered
357 isoforms with functional consequences (NMD status), 50% exhibited a significant reduction in
358 the NMD-sensitive isoforms upon FRG1 depletion (Fig. 2 A, B; Suppl. Fig. 2). Whereas only
359 one gene having NMD-sensitive isoform showed a significant increase, and the remaining
360 either showed no change in levels or non-significant change.

361 The influence of FRG1 on NMD efficiency was notably more pronounced in its
362 complete absence (Fig. 1 K, L). The knockout of FRG1 resulted in a substantial reduction in
363 NMD-sensitive isoforms for 60% of the top 10 genes with functionally significant altered
364 isoforms (NMD status). On the other hand, only two of these genes showed a significant
365 increase in NMD-sensitive isoforms, while the others exhibited either a non-significant
366 increase or no change (Fig. 2 C, D; Suppl. Fig. 3).

367 On a transcriptome-wide scale, comparing FRG1 depleted and knockout conditions, we
368 found more overlap in NMD-sensitive isoforms showing downregulation (18) than

369 upregulation (5) (Fig. 1 M). These findings provide evidence that FRG1 plays a crucial role in
370 regulating the elimination of key NMD targets.

371 **DUX4 regulates NMD via FRG1**

372 Feng et al. reported that DUX4, a transcriptional activator of FRG1, inhibits NMD [64–
373 66]. Mechanistically, we investigated whether FRG1 directly influences NMD, potentially
374 exceeding the impact of DUX4, or whether DUX4 exerts its effects on NMD independently of
375 FRG1. To ascertain this, we created a stable, inducible MCF7 cell line that expresses DUX4
376 upon doxycycline induction. As reported previously [65], increased levels of DUX4 led to
377 reduced NMD efficacy in MCF7 cells. Relative levels of luciferase signal obtained from the
378 NMD sensor construct was 1.5-fold higher in the DUX4 overexpressing cells, showing the
379 accumulation of PTC containing transcripts. However, NMD activity was restored (0.22-fold)
380 with less intensity of luciferase signal from the NMD sensor construct due to decreased
381 accumulation of PTC containing transcripts upon FRG1 depletion in DUX4 overexpressing
382 cells (Fig. 3). This data suggested that the DUX4-mediated inhibition of NMD can be via
383 FRG1.

384 **FRG1 dually regulates UPF1 expression, a central molecule in NMD**

385 Since previous studies demonstrated that DUX4 influences UPF1 protein levels [65]
386 and FRG1 affects the transcript levels of NMD factors [52], we investigated the impact of FRG1
387 on both UPF1 transcript and protein levels. We found an increase in UPF1 expression upon
388 FRG1 reduction, both at mRNA (fold change = 1.93) (Fig. 4 A) and protein levels (Fig. 4 B).
389 On the other hand, overexpression of FRG1 resulted in reduced UPF1 levels both at the RNA
390 level (fold change =0.8) (Fig. 4 C) and protein level (Fig. 4 D). Parallel to *in vitro* data, knockout
391 of frg1 in zebrafish resulted in increased upf1 expression (fold change=1.86) (Fig. 4 E). To
392 ascertain the specificity, we ectopically expressed FRG1 in the $frg1^{KO/KO}$ zebrafish model,

393 which showed reduction in upf1 expression (fold change=0.36) (Fig. 4 F). This data indicated
394 that FRG1 inversely regulates UPF1 expression.

395 **FRG1 Promotes Depletion of UPF1 Protein Independently of DUX4**

396 Our previous publication demonstrated the direct binding of FRG1 to the promoter region of
397 UPF1, establishing its role as a transcriptional regulator [52]. Building on these findings, we
398 investigated whether FRG1 exerts a direct effect on UPF1 protein levels, a phenomenon
399 previously reported in the context of DUX4. Consistent with earlier observations, DUX4
400 overexpression led to a marked reduction in UPF1 levels [65]. Interestingly, knockdown of
401 FRG1 in a DUX4-overexpressing background restored UPF1 expression, indicating that FRG1
402 directly contributes to the downregulation of UPF1 protein levels (Fig. 5A). To further
403 investigate this relationship, we overexpressed FRG1 in MCF7 cells, both with and without
404 DUX4 overexpression. Notably, FRG1 overexpression alone led to a marked reduction in UPF1
405 levels—comparable to the reduction seen in cells already engineered to overexpress DUX4
406 (Fig. 5B).

407 To explore the underlying mechanism, we examined the impact of proteasomal degradation.
408 We found that inhibiting proteasomal degradation in FRG1-overexpressing cells restored UPF1
409 levels (Fig. 5B). Treatment of MCF7 cells overexpressing FRG1 with 50 μM MG132 for 8, 12,
410 and 24 hours led to a time-dependent increase in UPF1 protein levels (Fig. 5C), confirming that
411 UPF1 degradation is mediated via the proteasome.

412 Collectively, these results provide strong evidence that FRG1 directly promotes UPF1 protein
413 depletion through a proteasome-dependent mechanism, independent of DUX4.

414 **FRG1 associates directly with UPF1 protein and promotes its ubiquitination and**
415 **degradation**

416 Next, we investigated whether FRG1 functions as part of the nonsense-mediated decay
417 machinery and negatively regulates UPF1 levels through direct interaction. Co-
418 immunoprecipitation assays, performed using reciprocal pulldown with either FRG1 or UPF1
419 antibodies, confirmed a protein-protein interaction between FRG1 and UPF1 (Fig. 6A–C).
420 These findings suggest that FRG1 serves as a structural component of the NMD complex.

421 To further investigate the underlying mechanism, we performed a co-immunoprecipitation-
422 based ubiquitination assay. FRG1 depletion led to a marked reduction in UPF1 ubiquitination,
423 accompanied by increased binding between UPF1 and FRG1. In contrast, ectopic expression
424 of FRG1 enhanced UPF1 ubiquitination while diminishing its interaction with FRG1 (Fig. 6D).
425 To validate these findings, we employed FRG1 knockout MCF7 cells and observed that ectopic
426 re-expression of FRG1 in this background successfully restored UPF1 ubiquitination,
427 confirming the role of FRG1 in regulating this process (Fig. 6E). Furthermore, a UPF1
428 pulldown assay performed under conditions of FRG1 overexpression—following treatment
429 with 50 μM MG132 for 8 hours—showed reduced levels of ubiquitinated UPF1 (Fig. 6F). This
430 finding confirms a proteasome-mediated degradation pathway.

431 Collectively, these results demonstrate that FRG1 regulates UPF1 stability by promoting its
432 ubiquitination and subsequent proteasomal degradation. Thus, FRG1 acts as a negative
433 regulator of UPF1 levels via a ubiquitin–proteasome mechanism (Fig. 5G–I).

434 **FRG1 is a structural component of the EJC and spliceosome complex**

435 FRG1 is reported as a structural component of spliceosomal C complex [49].
436 Overexpression of FRG1 leads to missplicing of transcripts [67]. Since splicing and nonsense-
437 mediated mRNA decay are closely interconnected processes [68,69], and since components of
438 the exon junction complex (EJC)—assembled during splicing—play a critical role in NMD
439 [70], we investigated whether FRG1 influences NMD by altering UPF1 levels or by disrupting

440 the structural integrity of the spliceosome and EJC. To explore this, we assessed the stability of
441 these complexes in FRG1-perturbed cells. PRP8, a core catalytic component of the
442 spliceosomal C complex [71], has been shown via cryo-electron microscopy (Cryo-EM) to
443 interact with FRG1 [51]. CWC22, a pre-mRNA splicing factor, bridges splicing and the EJC
444 [50]. We performed co-immunoprecipitation experiments on nuclear extracts from cells with
445 altered FRG1 expression, using an antibody against PRP8. Immunoblotting confirmed that
446 FRG1 interacts with both PRP8 and CWC22 in FRG1-overexpressing cells (Fig. 7 A).
447 However, in FRG1-deficient cells, the interaction between PRP8 and CWC22 remained
448 unaltered (Fig. 7 B). These findings suggest that although FRG1 is a structural component of
449 the human spliceosomal C complex, its absence does not compromise the complex's structural
450 integrity.

451 Next, we examined whether FRG1 affects the architecture of the EJC. We focused on
452 eIF4A3, a core EJC component [72], and UPF3B, a key factor in the NMD pathway. Co-IP
453 using an anti-eIF4A3 antibody on cytoplasmic extracts of FRG1-perturbed cells revealed
454 interactions between eIF4A3, FRG1, and UPF3B (Fig. 7 C). Notably, in FRG1-deficient cells,
455 the interaction between eIF4A3 and UPF3B was maintained (Fig. 7 D), indicating that FRG1
456 is not essential for EJC complex stability. To further probe the potential role of FRG1 in post-
457 transcriptional regulation, we performed polysome sucrose gradient fractionation followed by
458 immunoblotting. Remarkably, FRG1 co-sedimented with eIF4A3 across polysome fractions
459 (Fig. 7 E), suggesting a previously unrecognized association of FRG1 with actively translating
460 ribosomal complexes. This observation strongly supports a functional link between FRG1 and
461 the translation-coupled phase of EJC activity, hinting at a novel regulatory role for FRG1 in
462 mRNA surveillance or translation.

463 To validate the physical proximity suggested by co-sedimentation, we conducted a Proximity
464 Ligation Assay (PLA) to test whether FRG1 and eIF4A3 are spatially close enough to imply
465 direct or complex-mediated interaction. The PLA revealed distinct and abundant red
466 fluorescent puncta in cells, confirming that FRG1 and eIF4A3 are localized within less than 40
467 nm of each other—a range consistent with direct protein-protein interaction (Fig. 7 F). These
468 compelling findings strongly support the conclusion that FRG1 either directly binds eIF4A3 or
469 is stably associated within the same molecular complex. Altogether, this series of experiments
470 unveils an exciting new aspect of FRG1 biology and firmly establishes its integration into key
471 post-transcriptional gene regulatory pathways.

472 **Discussion:**

473 Research involving FRG1 has predominantly focussed on its association with FSHD
474 and muscle function [40,42,73]. Over the past decade, there has been a substantial increase in
475 understanding the additional roles of FRG1 in tumorigenesis and angiogenesis [43–46].
476 Although few studies have indicated that FRG1 expression levels affect the RNA biogenesis
477 of specific genes, but the exact mechanism is unknown [40,47,74]. The results presented in
478 this study sheds light on FRG1's role in modulating NMD processes, and its underlying
479 molecular mechanism suggesting the need for maintaining its optimal levels.

480 Our previous finding revealed that FRG1 depletion decreases the expression levels of
481 NMD factors such as MAGOH, PININ, ROD1, UPF3B, SMG1, and ICE1 [52]. Another study
482 demonstrated that ICE1 depletion reduces NMD efficiency, indirectly suggesting a potential
483 role for FRG1 in regulating NMD [38]. We observed that reduced FRG1 increased expression
484 level of UPF1 transcriptionally as well as translationally, thereby increasing NMD efficiency.
485 Thus, it is possible that FRG1, acting as a dual regulator of NMD genes may play a role in
486 stabilizing the NMD pathway, ensuring its robustness in quality control and regulating normal

487 gene expression. Previously, multiple studies have highlighted the role of NMD factors in
488 maintaining cellular homeostasis. The first indication of a buffering mechanism came from a
489 microarray profiling analysis on NMD deficient HeLa cells with depleted levels of the NMD
490 factor UPF1. In this, amongst the 195 significantly upregulated transcripts, mRNA encoding
491 the NMD factor SMG5 was identified [1]. In yet another study, SMG5 mRNA was found to be
492 regulated by the UPF3B-independent pathway [32]. Huang et al. demonstrated the presence of
493 a conserved feedback regulatory network wherein depletion of UPF1 in HeLa cells resulted in
494 upregulation of NMD factors- UPF2, UPF3B, SMG1, SMG5, SMG6, and SMG7 [75]. Study
495 by Yepiskoposyan et al. showed that long 3'UTRs of NMD substrate mRNAs (UPF1, SMG6,
496 and SMG7) trigger NMD, demonstrating autoregulation of NMD in human cells [76]. From all
497 of these studies, we may speculate that along with the aforementioned NMD factors, FRG1
498 might be a part of the feedback regulatory network, preserving the integrity of NMD. NMD
499 feedback loops are far more intricately regulated than currently understood. In future, genome-
500 wide analysis may help elucidate new NMD factors that might provide versatile and subtle
501 feedback control to achieve optimal NMD activity and protect NMD from perturbation.

502 DUX4 is a well-established transcriptional regulator of FRG1 [64,66]. Previously Feng
503 et al. reported that DUX4 reduces NMD efficiency triggering proteolytic degradation of UPF1
504 [65]. Consistent with this, our observation revealed that NMD efficiency is directly, but
505 inversely modulated by FRG1. We ascertained that DUX4-mediated NMD inhibition is
506 regulated by FRG1 expression. Delving into its molecular intricacy, we have shown that FRG1
507 mediates degradation of UPF1, which results in NMD inhibition. Thus, the close coupling
508 between DUX4 and FRG1 expression levels might be providing a regulatory mechanism to
509 maintain NMD homeostasis. However, it is yet to be determined if increased UPF1 protein
510 levels are primarily responsible for FRG1-induced NMD regulation or merely one of the
511 several contributing factors. Nonetheless, the expression levels of FRG1 in altering NMD

512 efficiency surpassing DUX4 may prove useful to gain insight into the biological relevance of
513 this mechanism. It is also tempting to speculate that FRG1-induced dysregulation of the
514 ubiquitin-proteasome system is responsible for triggering UPF1 protein degradation. The
515 precise mechanism by which FRG1 induces UPF1 proteolysis or whether FRG1 itself acts as
516 E3 ubiquitin ligase remains to be elucidated.

517 FRG1 serves as a structural component of spliceosome C complex by interacting with
518 PRP8 [51] and previous studies have linked increased FRG1 expression with abnormal splicing
519 [48,77]. Herein, we aimed to investigate whether it regulates NMD by being a structural
520 component of the Spliceosomal C complex. In this study, using FRG1 perturbed cell lines,
521 carrying out co-immunoprecipitation assays, we have established it as a structural component
522 of the Exon Junction Complex and Spliceosome Complex. However, we could also find that
523 FRG1's absence did not disrupt the interaction between CWC22 (a spliceosome molecule) and
524 PRP8 or eIF4A3 (core EJC molecule) and UPF3B. However, in this context, the finer
525 alterations in the spliceosome or exon junction complexes remain unexplored, leaving open the
526 possibility that FRG1 may influence their functionality. Alternatively, other NMD factors
527 might be compensating for the loss of FRG1 to maintain the structural integrity of the
528 complexes. This requires further validation. A comprehensive mass spectrometry analysis
529 conducted by Singh et al. [78] using immunoprecipitation from HEK293 cells expressing
530 FLAG-tagged eIF4A3 and mFLAG-Magoh, revealed a broad enrichment of EJC core and
531 peripheral components, along with spliceosomal proteins, heterogeneous nuclear
532 ribonucleoproteins (hnRNPs), ribosomal subunits, and serine/arginine-rich (SR) proteins.
533 These findings underscore the complex and multifunctional nature of the EJC and its dynamic
534 associations within the mRNP environment. In line with this, our polysome profiling data
535 provide compelling evidence for a potential interaction between FRG1 and eIF4A3, strongly
536 suggesting that FRG1 may associate with the EJC. This association further supports the

537 emerging view of FRG1 as a participant in post-transcriptional gene regulatory pathways,
538 possibly contributing to the coupling of splicing, translation, and mRNA surveillance
539 mechanisms. Future studies will be needed to address the degree of FRG1-dependent interplay
540 between splicing and NMD pathways.

541 In summary, this study provides mechanistic evidence that FRG1 inversely regulates
542 the NMD machinery. Crucially, we demonstrated that FRG1 directly modulates the NMD
543 pathway by influencing the ubiquitination of UPF1, an effect that surpasses the regulatory
544 impact of DUX4. The identification of FRG1 as an upstream regulator of NMD genes offers
545 valuable insights into the mechanisms underlying the fine-tuning of NMD. The findings from
546 this study pave the way for the development of novel therapeutic strategies targeting diseases
547 associated with FRG1 dysregulation.

548

549 **Abbreviations:**

550 FRG1 FSHD Region Gene 1

551 UPF1 Up-frameshift Protein 1

552 DUX4 Double homeobox 4

553 PRP8 Pre-mRNA processing factor 8

554 CWC22 Spliceosome associated protein homolog

555 UPF3B Up-frameshift Protein 3B

556 ICE1 Interactor of little elongation complex ELL subunit 1

557 MAGOH Mago Homolog

558 EJC Exon junction complex

SURF	SMG-1-Upf1-eRF1-eRF3 complex
GAPDH	Glyceraldehyde 3- phosphate dehydrogenase
DECID	Decay-inducing complex
SMG	PI3K related kinase
ROD1/PTBP3	Polypyrimidine Tract Binding Protein 3
Rbfox1	RNA-binding fox-1 homolog 1
FXR1	FMR1 autosomal homolog 1

Acknowledgement

Not Applicable

Funding

This work was supported by intramural funding from the National Institute of Science Education and Research (NISER), Department of Atomic Energy (DAE), Government of India (GOI). A.P., A.S., and S.T. received fellowship from NISER, DAE, GOI.

Author Contribution

A.P.: performed Western Blot, qRT-PCR, luciferase reporter assay, cell culture, co-immunoprecipitation, zebrafish experiments, formal analysis of data, writing- original draft and editing. T.M. performed cell culture, western blotting, co-immunoprecipitation, MG132 inhibitor treatments, and polysome assays, proximity ligation assay and contributed to editing the manuscript draft. A.S. and S.T.: analyzed RNA seq data. S.S.M.: helped in zebrafish

genotyping, maintaining zebrafish lines, and imaging work. R.K.S.: designed zebrafish-related experiments, carried out microinjection in zebrafish embryos, and reviewed the manuscript. M.D.: conceptualized the study, analysed the data, wrote and reviewed the manuscript, and acquired the funding.

Ethics Approval

All zebrafish-related experiments were performed following the protocol approved by Institutional Animal Ethics Committee (IAEC), ILS, Bhubaneswar under the protocol number ILS/IAEC-213-AH/APR-21 and ILS/IAEC-364-AH/SEPT-24.

Competing Interests

The authors declare that there are no competing interests associated with the manuscript.

Data Availability Statement

Data associated with this work are available upon request from the corresponding author.

References:

[1] J.T. Mendell, N.A. Sharifi, J.L. Meyers, F. Martinez-Murillo, H.C. Dietz, Nonsense surveillance regulates expression of diverse classes of mammalian transcripts and mutes genomic noise, Nat. Genet. 36 (2004) 1073–1078.

[2] L. Huang, M.F. Wilkinson, Regulation of nonsense-mediated mRNA decay, Wiley Interdiscip. Rev. RNA. 3 (2012) 807–828.

[3] V.S. Muir, A.P. Gasch, P. Anderson, The Substrates of Nonsense-Mediated mRNA

604 Decay in Caenorhabditis elegans., G3 (Bethesda). 8 (2018) 195–205.
605 https://doi.org/10.1534/g3.117.300254.

606 [4] R. Pulak, P. Anderson, mRNA surveillance by the Caenorhabditis elegans smg genes.,
607 Genes Dev. 7 (1993) 1885–1897.

608 [5] N. Wittkopp, E. Huntzinger, C. Weiler, J. Saulière, S. Schmidt, M. Sonawane, E.
609 Izaurralde, Nonsense-mediated mRNA decay effectors are essential for zebrafish
610 embryonic development and survival, Mol. Cell. Biol. 29 (2009) 3517–3528.

611 [6] L. Gardner, P.G. Corn, Hypoxic regulation of mRNA expression, Cell Cycle. 7 (2008)
612 1916–1924.

613 [7] D. Wang, J. Zavadil, L. Martin, F. Parisi, E. Friedman, D. Levy, H. Harding, D. Ron,
614 L.B. Gardner, Inhibition of nonsense-mediated RNA decay by the tumor
615 microenvironment promotes tumorigenesis, Mol. Cell. Biol. 31 (2011) 3670–3680.

616 [8] C.H. Lou, A. Shao, E.Y. Shum, J.L. Espinoza, L. Huang, R. Karam, M.F. Wilkinson,
617 Posttranscriptional control of the stem cell and neurogenic programs by the nonsense-
618 mediated RNA decay pathway, Cell Rep. 6 (2014) 748–764.

619 [9] C.-H. Lou, J. Dumdie, A. Goetz, E.Y. Shum, D. Brafman, X. Liao, S. Mora-Castilla,
620 M. Ramaiah, H. Cook-Andersen, L. Laurent, Nonsense-mediated RNA decay
621 influences human embryonic stem cell fate, Stem Cell Reports. 6 (2016) 844–857.

622 [10] D.R. McIlwain, Q. Pan, P.T. Reilly, A.J. Elia, S. McCracken, A.C. Wakeham, A. Itie-
623 Youten, B.J. Blencowe, T.W. Mak, Smg1 is required for embryogenesis and regulates
624 diverse genes via alternative splicing coupled to nonsense-mediated mRNA decay,
625 Proc. Natl. Acad. Sci. 107 (2010) 12186–12191.

626 [11] S.M. Medghalchi, P.A. Frischmeyer, J.T. Mendell, A.G. Kelly, A.M. Lawler, H.C.
627 Dietz, Rent1, a trans-effector of nonsense-mediated mRNA decay, is essential for
628 mammalian embryonic viability, Hum. Mol. Genet. 10 (2001) 99–105.

629 [12] L.A. Thoren, G.A. Nørgaard, J. Weischenfeldt, J. Waage, J.S. Jakobsen, I. Damgaard,
630 F.C. Bergström, A.M. Blom, R. Borup, H.C. Bisgaard, UPF2 is a critical regulator of
631 liver development, function and regeneration, PLoS One. 5 (2010) e11650.

632 [13] L. Linde, S. Boelz, G. Neu-Yilik, A.E. Kulozik, B. Kerem, The efficiency of nonsense-
633 mediated mRNA decay is an inherent character and varies among different cells, Eur.
634 J. Hum. Genet. 15 (2007) 1156–1162.

635 [14] F. Usuki, A. Yamashita, I. Kashima, I. Higuchi, M. Osame, S. Ohno, Specific
636 inhibition of nonsense-mediated mRNA decay components, SMG-1 or Upf1, rescues
637 the phenotype of Ullrich disease fibroblasts, Mol. Ther. 14 (2006) 351–360.

638 [15] L.A. Jolly, C.C. Homan, R. Jacob, S. Barry, J. Gecz, The UPF3B gene, implicated in
639 intellectual disability, autism, ADHD and childhood onset schizophrenia regulates
640 neural progenitor cell behaviour and neuronal outgrowth, Hum. Mol. Genet. 22 (2013)
641 4673–4687.

642 [16] F. Laumonnier, C. Shoubridge, C. Antar, L.S. Nguyen, H. Van Esch, T. Kleefstra, S.
643 Briault, J.P. Fryns, B. Hamel, J. Chelly, Mutations of the UPF3B gene, which encodes
644 a protein widely expressed in neurons, are associated with nonspecific mental
645 retardation with or without autism, Mol. Psychiatry. 15 (2010) 767–776.

646 [17] X. Xu, L. Zhang, P. Tong, G. Xun, W. Su, Z. Xiong, T. Zhu, Y. Zheng, S. Luo, Y.
647 Pan, Exome sequencing identifies UPF3B as the causative gene for a Chinese non-
648 syndrome mental retardation pedigree, Clin. Genet. 83 (2013) 560–564.

649 [18] J.L. Johnson, L. Stoica, Y. Liu, P.J. Zhu, A. Bhattacharya, S.A. Buffington, R. Huq,
650 N.T. Eissa, O. Larsson, B.T. Porse, Inhibition of Upf2-dependent nonsense-mediated
651 decay leads to behavioral and neurophysiological abnormalities by activating the
652 immune response, Neuron. 104 (2019) 665–679.

653 [19] L.S. Nguyen, H.-G. Kim, J.A. Rosenfeld, Y. Shen, J.F. Gusella, Y. Lacassie, L.C.
654 Layman, L.G. Shaffer, J. Gécz, Contribution of copy number variants involving
655 nonsense-mediated mRNA decay pathway genes to neuro-developmental disorders,
656 Hum. Mol. Genet. 22 (2013) 1816–1825.

657 [20] J. El-Bchiri, A. Guilloux, P. Dartigues, E. Loire, D. Mercier, O. Buhard, I. Sobhani, P.
658 De la Grange, D. Auboeuf, F. Praz, Nonsense-mediated mRNA decay impacts MSI-
659 driven carcinogenesis and anti-tumor immunity in colorectal cancers, PLoS One. 3
660 (2008) e2583.

661 [21] T.J. Pugh, O. Morozova, E.F. Attiyeh, S. Asgharzadeh, J.S. Wei, D. Auclair, S.L.
662 Carter, K. Cibulskis, M. Hanna, A. Kiezun, The genetic landscape of high-risk
663 neuroblastoma, Nat. Genet. 45 (2013) 279–284.

664 [22] C. Liu, R. Karam, Y. Zhou, F. Su, Y. Ji, G. Li, G. Xu, L. Lu, C. Wang, M. Song, The
665 UPF1 RNA surveillance gene is commonly mutated in pancreatic adenosquamous
666 carcinoma, Nat. Med. 20 (2014) 596–598.

667 [23] J. Lu, T.-D. Plank, F. Su, X. Shi, C. Liu, Y. Ji, S. Li, A. Huynh, C. Shi, B. Zhu, The
668 nonsense-mediated RNA decay pathway is disrupted in inflammatory myofibroblastic
669 tumors, J. Clin. Invest. 126 (2016) 3058–3062.

670 [24] T.L. Roberts, U. Ho, J. Luff, C.S. Lee, S.H. Apte, K.P.A. MacDonald, L.J. Raggat,
671 A.R. Pettit, C.A. Morrow, M.J. Waters, Smg1 haploinsufficiency predisposes to tumor

672 formation and inflammation, Proc. Natl. Acad. Sci. 110 (2013) E285–E294.

673 [25] Y. He, M.M. Sun, G.G. Zhang, J. Yang, K.S. Chen, W.W. Xu, B. Li, Targeting
674 PI3K/Akt signal transduction for cancer therapy, Signal Transduct. Target. Ther. 6
675 (2021) 425.

676 [26] P.S. Mundi, J. Sachdev, C. McCourt, K. Kalinsky, AKT in cancer: new molecular
677 insights and advances in drug development, Br. J. Clin. Pharmacol. 82 (2016) 943–
678 956.

679 [27] F. Rascio, F. Spadaccino, M.T. Rocchetti, G. Castellano, G. Stallone, G.S. Netti, E.
680 Ranieri, The pathogenic role of PI3K/AKT pathway in cancer onset and drug
681 resistance: an updated review, Cancers (Basel). 13 (2021) 3949.

682 [28] J.C. Reddy, J.C. Morris, J. Wang, M.A. English, D.A. Haber, Y. Shi, J.D. Licht, WT1-
683 mediated transcriptional activation is inhibited by dominant negative mutant proteins,
684 J. Biol. Chem. 270 (1995) 10878–10884.

685 [29] L. Perrin-Vidoz, O.M. Sinilnikova, D. Stoppa-Lyonnet, G.M. Lenoir, S. Mazoyer, The
686 nonsense-mediated mRNA decay pathway triggers degradation of most BRCA1
687 mRNAs bearing premature termination codons, Hum. Mol. Genet. 11 (2002) 2805–
688 2814.

689 [30] O. Anczuków, M.D. Ware, M. Buisson, A.B. Zetoune, D. Stoppa-Lyonnet, O.M.
690 Sinilnikova, S. Mazoyer, Does the nonsense-mediated mRNA decay mechanism
691 prevent the synthesis of truncated BRCA1, CHK2, and p53 proteins?, Hum. Mutat. 29
692 (2008) 65–73.

693 [31] N.H. Gehring, J.B. Kunz, G. Neu-Yilik, S. Breit, M.H. Viegas, M.W. Hentze, A.E.

694 Kulozik, Exon-junction complex components specify distinct routes of nonsense-
695 mediated mRNA decay with differential cofactor requirements, Mol. Cell. 20 (2005)
696 65–75.

697 [32] W. Chan, L. Huang, J.P. Gudikote, Y. Chang, J.S. Imam, J.A. MacLean, M.F.
698 Wilkinson, An alternative branch of the nonsense-mediated decay pathway, EMBO J.
699 26 (2007) 1820–1830.

700 [33] I. Kashima, A. Yamashita, N. Izumi, N. Kataoka, R. Morishita, S. Hoshino, M. Ohno,
701 G. Dreyfuss, S. Ohno, Binding of a novel SMG-1–Upf1–eRF1–eRF3 complex (SURF)
702 to the exon junction complex triggers Upf1 phosphorylation and nonsense-mediated
703 mRNA decay, Genes Dev. 20 (2006) 355–367.

704 [34] L. Unterholzner, E. Izaurralde, SMG7 acts as a molecular link between mRNA
705 surveillance and mRNA decay, Mol. Cell. 16 (2004) 587–596.

706 [35] B. Loh, S. Jonas, E. Izaurralde, The SMG5–SMG7 heterodimer directly recruits the
707 CCR4–NOT deadenylase complex to mRNAs containing nonsense codons via
708 interaction with POP2, Genes Dev. 27 (2013) 2125–2138.

709 [36] J. Lykke-Andersen, Identification of a human decapping complex associated with
710 hUpf proteins in nonsense-mediated decay, Mol. Cell. Biol. 22 (2002) 8114–8121.

711 [37] T.F. Brazão, J. Demmers, W. van IJcken, J. Strouboulis, M. Fornerod, L. Romão, F.G.
712 Grosveld, A new function of ROD1 in nonsense-mediated mRNA decay, FEBS Lett.
713 586 (2012) 1101–1110.

714 [38] T.D. Baird, K.C.-C. Cheng, Y.-C. Chen, E. Buehler, S.E. Martin, J. Inglese, J.R. Hogg,
715 ICE1 promotes the link between splicing and nonsense-mediated mRNA decay, Elife.

716 7 (2018) e33178.

717 [39] D. Longman, N. Hug, M. Keith, C. Anastasaki, E.E. Patton, G. Grimes, J.F. Caceres,
718 DHX34 and NBAS form part of an autoregulatory NMD circuit that regulates
719 endogenous RNA targets in human cells, zebrafish and Caenorhabditis elegans,
720 Nucleic Acids Res. 41 (2013) 8319–8331.

721 [40] D. Gabellini, G. D'Antona, M. Moggio, A. Prelle, C. Zecca, R. Adami, B. Angeletti, P.
722 Ciscato, M.A. Pellegrino, R. Bottinelli, Facioscapulohumeral muscular dystrophy in
723 mice overexpressing FRG1, Nature. 439 (2006) 973–977.

724 [41] J.C.T. van Deutekom, R.J.L.F. Lemmers, P.K. Grewal, M. van Geel, S. Romberg, H.G.
725 Dauwerse, T.J. Wright, G.W. Padberg, M.H. Hofker, J.E. Hewitt, Identification of the
726 first gene (FRG1) from the FSHD region on human chromosome 4q35, Hum. Mol.
727 Genet. 5 (1996) 581–590.

728 [42] S.J. Feeney, M.J. McGrath, A. Sriratana, S.M. Gehrig, G.S. Lynch, C.E. D'Arcy, J.T.
729 Price, C.A. McLean, R. Tupler, C.A. Mitchell, FHL1 reduces dystrophy in transgenic
730 mice overexpressing FSHD muscular dystrophy region gene 1 (FRG1), PLoS One. 10
731 (2015) e0117665.

732 [43] A. Tiwari, N. Pattnaik, A. Mohanty Jaiswal, M. Dixit, Increased FSHD region gene1
733 expression reduces in vitro cell migration, invasion, and angiogenesis, ex vivo
734 supported by reduced expression in tumors, Biosci. Rep. 37 (2017).

735 [44] A. Tiwari, B. Mukherjee, M.K. Hassan, N. Pattanaik, A.M. Jaiswal, M. Dixit, Reduced
736 FRG1 expression promotes prostate cancer progression and affects prostate cancer cell
737 migration and invasion, BMC Cancer. 19 (2019) 1–15.

738 [45] B. Mukherjee, A. Tiwari, A. Palo, N. Pattnaik, S. Samantara, M. Dixit, Reduced
739 expression of FRG1 facilitates breast cancer progression via GM-CSF/MEK-ERK axis
740 by abating FRG1 mediated transcriptional repression of GM-CSF, Cell Death Discov.
741 8 (2022) 442.

742 [46] B. Mukherjee, P. Brahma, T. Mohapatra, S. Chawla, M. Dixit, Reduced FRG1
743 expression promotes angiogenesis via activation of the FGF2-mediated ERK/AKT
744 pathway, Wiley Online Library, 2023.

745 [47] C.-Y.J. Sun, S. Van Koningsbruggen, S.W. Long, K. Straasheijm, R. Klooster, T.I.
746 Jones, M. Bellini, L. Levesque, W.M. Brieher, S.M. Van Der Maarel,
747 Facioscapulohumeral muscular dystrophy region gene 1 is a dynamic RNA-associated
748 and actin-bundling protein, J. Mol. Biol. 411 (2011) 397–416.

749 [48] M. Pistoni, L. Shiue, M.S. Cline, S. Bortolanza, M.V. Neguembor, A. Xynos, M. Ares
750 Jr, D. Gabellini, Rbfox1 downregulation and altered calpain 3 splicing by FRG1 in a
751 mouse model of Facioscapulohumeral muscular dystrophy (FSHD), PLoS Genet. 9
752 (2013) e1003186.

753 [49] A. Hegele, A. Kamburov, A. Grossmann, C. Sourlis, S. Wowro, M. Weimann, C.L.
754 Will, V. Pena, R. Lührmann, U. Stelzl, Dynamic protein-protein interaction wiring of
755 the human spliceosome, Mol. Cell. 45 (2012) 567–580.

756 [50] A.-L. Steckelberg, V. Boehm, A.M. Gromadzka, N.H. Gehring, CWC22 connects pre-
757 mRNA splicing and exon junction complex assembly, Cell Rep. 2 (2012) 454–461.

758 [51] K. Bertram, L. El Ayoubi, O. Dybkov, D.E. Agafonov, C.L. Will, K. Hartmuth, H.
759 Urlaub, B. Kastner, H. Stark, R. Lührmann, Structural Insights into the Roles of
760 Metazoan-Specific Splicing Factors in the Human Step 1 Spliceosome, Mol. Cell. 80

761 (2020) 127–139.

762 [52] A. Palo, S.A. Patel, B. Sahoo, T.K. Chowdary, M. Dixit, FRG1 is a direct
763 transcriptional regulator of nonsense-mediated mRNA decay genes, Genomics. 115
764 (2023) 110539.

765 [53] G.K. Varshney, W. Pei, M.C. LaFave, J. Idol, L. Xu, V. Gallardo, B. Carrington, K.
766 Bishop, M. Jones, M. Li, High-throughput gene targeting and phenotyping in zebrafish
767 using CRISPR/Cas9, Genome Res. 25 (2015) 1030–1042.

768 [54] C. Thisse, B. Thisse, High-resolution in situ hybridization to whole-mount zebrafish
769 embryos, Nat. Protoc. 3 (2008) 59–69.

770 [55] R. Patro, G. Duggal, M.I. Love, R.A. Irizarry, C. Kingsford, Salmon provides fast and
771 bias-aware quantification of transcript expression, Nat. Methods. 14 (2017) 417–419.

772 [56] C. Soneson, M.I. Love, M.D. Robinson, Differential analyses for RNA-seq: transcript-
773 level estimates improve gene-level inferences, F1000Research. 4 (2015).

774 [57] K. Vitting-Seerup, A. Sandelin, The landscape of isoform switches in human cancers,
775 Mol. Cancer Res. 15 (2017) 1206–1220.

776 [58] K. Vitting-Seerup, B.T. Porse, A. Sandelin, J. Waage, spliceR: an R package for
777 classification of alternative splicing and prediction of coding potential from RNA-seq
778 data, BMC Bioinformatics. 15 (2014) 1–7.

779 [59] J. Weischenfeldt, J. Waage, G. Tian, J. Zhao, I. Damgaard, J.S. Jakobsen, K.
780 Kristiansen, A. Krogh, J. Wang, B.T. Porse, Mammalian tissues defective in nonsense-
781 mediated mRNA decay display highly aberrant splicing patterns, Genome Biol. 13
782 (2012) 1–19.

783 [60] W. Huber, V.J. Carey, R. Gentleman, S. Anders, M. Carlson, B.S. Carvalho, H.C.
784 Bravo, S. Davis, L. Gatto, T. Girke, Orchestrating high-throughput genomic analysis
785 with Bioconductor, Nat. Methods. 12 (2015) 115–121.

786 [61] M.E. Ritchie, B. Phipson, D.I. Wu, Y. Hu, C.W. Law, W. Shi, G.K. Smyth, limma
787 powers differential expression analyses for RNA-sequencing and microarray studies,
788 Nucleic Acids Res. 43 (2015) e47–e47.

789 [62] S. Anders, A. Reyes, W. Huber, Detecting differential usage of exons from RNA-seq
790 data, Nat. Preced. (2012) 1.

791 [63] Z. Gu, R. Eils, M. Schlesner, Complex heatmaps reveal patterns and correlations in
792 multidimensional genomic data, Bioinformatics. 32 (2016) 2847–2849.

793 [64] G. Ferri, C.H. Huichalaf, R. Caccia, D. Gabellini, Direct interplay between two
794 candidate genes in FSHD muscular dystrophy, Hum. Mol. Genet. 24 (2015) 1256–
795 1266.

796 [65] Q. Feng, L. Snider, S. Jagannathan, R. Tawil, S.M. van der Maarel, S.J. Tapscott, R.K.
797 Bradley, A feedback loop between nonsense-mediated decay and the retrogene DUX4
798 in facioscapulohumeral muscular dystrophy, Elife. 4 (2015) e04996.

799 [66] A. Palo, S.A. Patel, S. Shubhanjali, M. Dixit, Dynamic interplay of Sp1, YY1, and
800 DUX4 in regulating FRG1 transcription with intricate balance, Biochim. Biophys.
801 Acta (BBA)-Molecular Basis Dis. (2024) 167636.

802 [67] M. Pistoni, C. Ghigna, D. Gabellini, Alternative splicing and muscular dystrophy,
803 RNA Biol. 7 (2010) 441–452.

804 [68] L.F. Lareau, A.N. Brooks, D.A.W. Soergel, Q. Meng, S.E. Brenner, The coupling of

805 alternative splicing and nonsense-mediated mRNA decay, Altern. Splicing
806 Postgenomic Era. (2007) 190–211.

807 [69] A. Zhuravskaya, K. Yap, F. Hamid, E. V Makeyev, Alternative splicing coupled to
808 nonsense-mediated decay coordinates downregulation of non-neuronal genes in
809 developing mouse neurons, Genome Biol. 25 (2024) 162.

810 [70] N.H. Gehring, S. Lamprinaki, M.W. Hentze, A.E. Kulozik, The hierarchy of exon-
811 junction complex assembly by the spliceosome explains key features of mammalian
812 nonsense-mediated mRNA decay, PLoS Biol. 7 (2009) e1000120.

813 [71] R.J. Grainger, J.D. Beggs, Prp8 protein: at the heart of the spliceosome, Rna. 11 (2005)
814 533–557.

815 [72] C.C. Chan, J. Dostie, M.D. Diem, W. Feng, M. Mann, J. Rappsilber, G. Dreyfuss,
816 eIF4A3 is a novel component of the exon junction complex, Rna. 10 (2004) 200–209.

817 [73] M.L. Hanel, R.D. Wuebbles, P.L. Jones, Muscular dystrophy candidate gene FRG1 is
818 critical for muscle development, Dev. Dyn. 238 (2009) 1502–1512.

819 [74] S. van Koningsbruggen, K.R. Straasheijm, E. Sterrenburg, N. de Graaf, H.G.
820 Dauwerse, R.R. Frants, S.M. van der Maarel, FRG1P-mediated aggregation of proteins
821 involved in pre-mRNA processing, Chromosoma. 116 (2007) 53–64.

822 [75] L. Huang, C.-H. Lou, W. Chan, E.Y. Shum, A. Shao, E. Stone, R. Karam, H.-W. Song,
823 M.F. Wilkinson, RNA homeostasis governed by cell type-specific and branched
824 feedback loops acting on NMD, Mol. Cell. 43 (2011) 950–961.

825 [76] H. Yepiskoposyan, F. Aeschimann, D. Nilsson, M. Okoniewski, O. Mühlemann,
826 Autoregulation of the nonsense-mediated mRNA decay pathway in human cells, Rna.

827 17 (2011) 2108–2118.

828 [77] V. Sancisi, E. Germinario, A. Esposito, E. Morini, S. Peron, M. Moggio, G. Tomelleri,
829 D. Danieli-Betto, R. Tupler, Altered Tnnt3 characterizes selective weakness of fast
830 fibers in mice overexpressing FSHD region gene 1 (FRG1), Am. J. Physiol. Integr.
831 Comp. Physiol. 306 (2014) R124–R137.

832 [78] Mabin, J. W., Woodward, L. A., Patton, R. D., Yi, Z., Jia, M., Wysocki, V. H., ... &
833 Singh, G. (2018). The exon junction complex undergoes a compositional switch that
834 alters mRNP structure and nonsense-mediated mRNA decay activity. *Cell*
835 *reports*, *25*(9), 2431-2446.

836

837 **Figure Legends:**

838 **Figure 1**. **FRG1 depletion increases NMD efficiency**. **(A–C)** Bar graphs depict relative
839 luciferase activity in the NMD reporter under varying conditions of FRG1 manipulation:
840 knockdown **(A)**, knockout **(B)**, and overexpression **(C)**. The figure uses the following
841 abbreviations for labeling: Control_Sc (Control_Scrambled), Control_EV (Control_Empty
842 Vector), WT (Wild Type), FRG1_KD (FRG1 Knockdown), FRG1_KO (FRG1 Knockout), and
843 FRG1_Ex (FRG1 Overexpression). **(D-G)** Expression of frg1 in wild-type (WT) and frg1
844 knockout zebrafish at different time points. Image **(D)** and **(E)** show frg1 expression in WT
845 and frg1 knockout embryos, respectively, at 24 hours post-fertilization (hpf). Image **(F)** and
846 **(G)** depict frg1 expression in WT and frg1 knockout embryos, respectively, at 48 hpf. **(H)** The
847 bar graph illustrates relative luciferase activity from NMD reporter in the zebrafish embryos
848 having different frg1 expression conditions [wild type (WT), homozygous frg1 knockout
849 (frg1_HOMO_KO), and FRG1 overexpression on frg1 homozygous knockout background

850 (frg1_HOMO_KO+Ex)] at 48 hpf. **(I, K)** Bar graph depict the proportion of transcripts
851 containing PTCs in MCF7 cell line having FRG1 knockdown **(I)** and knockout (K). The
852 analysis was conducted using IsoformSwitchAnalyzeR on RNA-Seq data from MCF7 cells
853 following FRG1 depletion. (J, L) The panels show Volcano plots, illustrating the change in
854 isoform fraction (dIF) plotted against the −log10 of the q-value, highlighting differential
855 transcript usage in FRG1-depleted RNA-Seq data from MCF7 cells. Isoforms are classified
856 based on GENCODE (release 47) annotations: those with PTCs are marked in red (TRUE),
857 with regular stop codons in blue (FALSE), and isoforms lacking an annotated open reading
858 frame in gray (NA). The lower panels present density plots showing the distribution of filtered
859 isoforms relative to thresholds of $|dIF| > 0.1$ and q-value < 0.05. Q-values were calculated using
860 IsoformSwitchAnalyzeR's DEXSeq-based statistical framework. (M) The UpSet plot
861 illustrates the overlap of upregulated and downregulated isoforms containing PTCs identified
862 in the FRG1 knockdown (KD) and knockout (KO) RNA-Seq datasets. Experiments were
863 performed in triplicate. Results are presented as mean ± SD. ns- non-significant; * represents
864 p-value ≤ 0.05; ** represents p-value ≤ 0.01; **** represents p-value ≤ 0.0001.

865 **Figure 2. NMD-sensitive isoform levels upon FRG1 depletion. (A-B)** The figure shows the
866 isoform expression profile plots displaying isoform structures with annotated Ensembl IDs,
867 isoform expression, and isoform fractions for genes ARL8B **(A)** and IRF9 **(B)**, in FRG1 knock
868 down (**FRG1_KD**) set. **(C-D).** The figure shows the isoform expression profile plots
869 illustrating the isoform structures with annotated Ensembl IDs, isoform expression levels, and
870 isoform fractions for the genes OSBPL7 **(panel C)** and REEP4 **(panel D)** in the FRG1
871 knockout (FRG1_KO) dataset. Red boxes highlight the NMD-sensitive isoforms of the
872 respective genes. (The remaining top 8 genes exhibiting isoform switching are shown in Suppl.
873 Fig. 2 and 3 for FRG1 knockdown and knockout, respectively.)

874 **Figure 3. DUX4 modulates NMD efficiency via FRG1.** The bar graph shows relative
875 luciferase signal from NMD reporter plasmid under DUX4 and FRG1 perturbed conditions
876 [DUX4 uninduced (DUX4_UI), DUX4 expression induced (DUX4_I), DUX4 expression
877 induced and FRG1 knockdown (DUX4_I+FRG1_KD)] in MCF7 cells. Experiments were
878 performed in triplicate. Results are presented as mean ± SD. * represents p-value ≤ 0.05; **
879 represents p-value ≤ 0.01.

880 **Figure 4. FRG1 expression perturbation alters UPF1 expression**. **(A-B)** qRT-PCR
881 expression data **(A)** and Western blot images **(B)** showing UPF1 expression upon FRG1
882 depletion in MCF7 cells. **(C-D)** qRT-PCR expression data **(C)** and Western blot images **(D)**
883 showing UPF1 levels upon ectopic FRG1 expression in MCF7 cells. Here are the details of
884 abbreviations used in labeling: FRG1 knockdown (FRG1_KD), FRG1 overexpression
885 (FRG1_Ex), Control_Scrambled (Control_Sc)/ Control_Empty Vector (Control_EV).
886 Experiments were performed in triplicate. **(E)** Bar graph depicts the qRT-PCR based
887 expression levels of upf1 following knockout of frg1 (frg1_ko) in zebrafish. (F) Bar graph
888 shows the qRT-PCR based expression levels of upf1 following ectopic expression of FRG1
889 under frg1 knockout background (frg1_ko+Ex) in zebrafish. Results are presented as mean ±
890 SD. ns- nonsignificant; * represents p-value ≤ 0.05; *** represents p-value ≤ 0.001; ****
891 represents p-value ≤ 0.0001.

892 **Figure 5. FRG1 Facilitates UPF1 Protein Reduction Independent of DUX4 Activity. (A)**
893 Western blot analysis illustrating UPF1 protein levels in MCF7 cells under various conditions:
894 lane-2 shows the effect of DUX4 expression (DUX4_I), while subsequent lanes depict the
895 impact of FRG1 knockdown in the presence of DUX4 expression (DUX4_I + FRG1_KD). **(B)**
896 Western blot showing time-dependent effect of MG132 treatment (8, 12, and 24 h) on UPF1
897 ubiquitination in FRG1-overexpressing MCF7 cells. UPF1 was immunoprecipitated and

898 probed with anti-ubiquitin antibody to assess polyubiquitination levels. (displays representative
899 Western blot results showing UPF1 expression in MCF7 cells with endogenous DUX4
900 expression (DUX4_UI) and overexpression of FRG1 (FRG1_Ex), following treatment with
901 MG132 (50 μM) (Lane-2). Lane-3 illustrates UPF1 expression in MCF7 cells co-expressing
902 DUX4 and FRG1 (DUX4_I + FRG1_Ex). Experiments were performed in triplicate. Results
903 are presented as mean ± SD. ns- nonsignificant; *** represents p-value ≤ 0.001; ****
904 represents p-value ≤ 0.0001.C)

905 **Figure 6. FRG1 interacts with UPF1 and mediates its proteasomal degradation**. **(A-B)** Co-
906 immunoprecipitation with UPF1 **(A)** and FRG1 **(B)** antibodies and representative Western
907 blots showing interaction of FRG1 with UPF1 in MCF7 cell line. **(C)** Immunoblot analysis of
908 a quantitative co-immunoprecipitation assay using UPF1 antibody demonstrates UPF1
909 ubiquitination under conditions of FRG1 knockdown (FRG1_KD, left three lanes) and FRG1
910 overexpression (FRG1_Ex, right three lanes). Co-immunoprecipitation with IgG was used as
911 negative control. **(D-F)** Validation of FRG1-dependent regulation of UPF1 ubiquitination and
912 stability via the proteasome pathway. **(D)** Immunoblot analysis of a quantitative co-
913 immunoprecipitation assay using UPF1 antibody demonstrates UPF1 ubiquitination (UB)
914 under conditions of FRG1 endogenous levels (FRG1_WT, left three lanes) and FRG1
915 knockout (FRG1_KO, right three lanes). Co-immunoprecipitation with IgG was used as
916 negative control. **(E)** Immunoblot analysis of a quantitative co-immunoprecipitation assay
917 using UPF1 antibody shows comparison of UPF1 ubiquitination (UB) in FRG1 knockout
918 background (FRG1_KO left three lanes) with reintroduction of FRG1 in the knockout
919 background (FRG1_KO+Oex, right three lanes) . **(F)** Immunoblot analysis of a quantitative
920 co-immunoprecipitation assay using a UPF1 antibody compares UPF1 ubiquitination (UB)
921 levels in FRG1-overexpressing cells (FRG1_Ex, left three lanes) with those in FRG1-

922 overexpressing cells subjected to an 8-hour treatment with 50 μM MG132
923 (FRG1_OEX_MG132 TRT).

924 **Figure 7. Interaction of FRG1 with Spliceosome and Exon Junction Complex**. **(A-B)**
925 Representative Western blots demonstrating co-immunoprecipitation with the PRP8 antibody
926 in the nuclear extracts (NE) of MCF7 cells. Panel **(A)** shows results from cells with FRG1
927 overexpression, while panel **(B)** displays findings from cells with FRG1 knockdown. Co-
928 immunoprecipitation with IgG was used as a negative control. **(C-D)** Representative Western
929 blots illustrating co-immunoprecipitation with the eIF4A3 antibody in the cytoplasmic extract
930 (CE) of MCF7 cells with ectopic FRG1 expression **(C)** and reduced FRG1 expression **(D)**. Co-
931 immunoprecipitation with IgG was used as a negative control. **(E)** Upper panel: Sucrose
932 gradient fractionation of cytoplasmic extracts from MCF7 cells. The polysome profile displays
933 relative absorbance at 254 nm across a 20–40% sucrose gradient, Lower panel: Immunoblot
934 analysis of gradient fractions using antibodies against FRG1 and eIF4A3. Immunoblot lanes
935 corresponding to the 40S, 60S, 80S ribosomal subunits, and polysome peaks are indicated. **(F)**
936 Proximity Ligation Assay (PLA) performed using antibodies against FRG1 and eIF4A3.
937 Representative confocal images of MCF7 cells (acquired at 60× magnification) are shown in
938 the upper panel. Red puncta indicate positive PLA signals, representing protein–protein
939 proximity (<40 nm), suggestive of a potential interaction. Nuclei are counterstained with DAPI
940 (blue). The lower panel shows 100× magnified views of the PLA puncta, emphasizing the
941 specificity of the observed interaction.

942 **Supplementary Figure 1. Screening of frg1 knockout AB strain zebrafish. (A-B)** Agarose
943 gel images showing amplified frg1 exon-1(153 bp) in wild type (WT), heterozygous
944 (HETERO), and homozygous (HOMO) zebrafish embryos **(A)** Agarose gel image showing
945 amplified frg1 exon-1(153 bp) in wild type (WT) but not in homozygous (HOMO) zebrafish

946 embryos. **(C-F)** show image of zebrafish embryos having expression of frg1 in wild type (WT)
947 **(C)** and frg1 knockout (frg1) **(D)** conditions at 24 hours post fertilization (hpf) stage. **(E-F)**
948 show image of zebrafish embryos having expression of frg1 in wild type (WT) **(E)** and frg1
949 knockout (frg1) **(F)** conditions at 48 hours post fertilization (hpf) stage.

950 **Supplementary Figure 2. NMD-sensitive isoform levels upon FRG1 knockdown.** The
951 figure shows the isoform expression profile plots displaying isoform structures in the upper
952 panel along with the annotated ensembl IDs. The lower panel displays isoform expression and
953 isoform fraction of NUB1 **(A)**, ACOX1 **(B)**, XPO5 **(C)**, ZMYND11 **(D)**, LZTFL1 **(E)**, SLMAP
954 **(F)**, RAD51D **(G)** and TRIM47 **(H)** undergoing isoform switching upon FRG1 depletion
955 (FRG1_KD vs control). Red box indicates the NMD-sensitive isoforms of the corresponding
956 genes.

957 **Supplementary Figure 3. NMD-sensitive isoform levels upon FRG1 knockout.** The figure
958 shows the isoform expression profile plot displaying isoform structures in the upper panel along
959 with the annotated ensembl IDs. The lower panel displays isoform expression and isoform
960 fraction of ERGICI1 **(A)**, ZW10 **(B)**, OSBPL7 **(C)**, REEP4 **(D)**, MRPL22 **(E)**, DTWD2 **(F)**,
961 OAS2 **(G)**, DRAM1 **(H)**, BMERB1 **(I)** and WDR20 **(J)** undergoing isoform switching in the
962 absence of FRG1 (FRG1_KO vs control). Red box indicates the NMD-sensitive isoforms of
963 the corresponding genes.

Figure 1

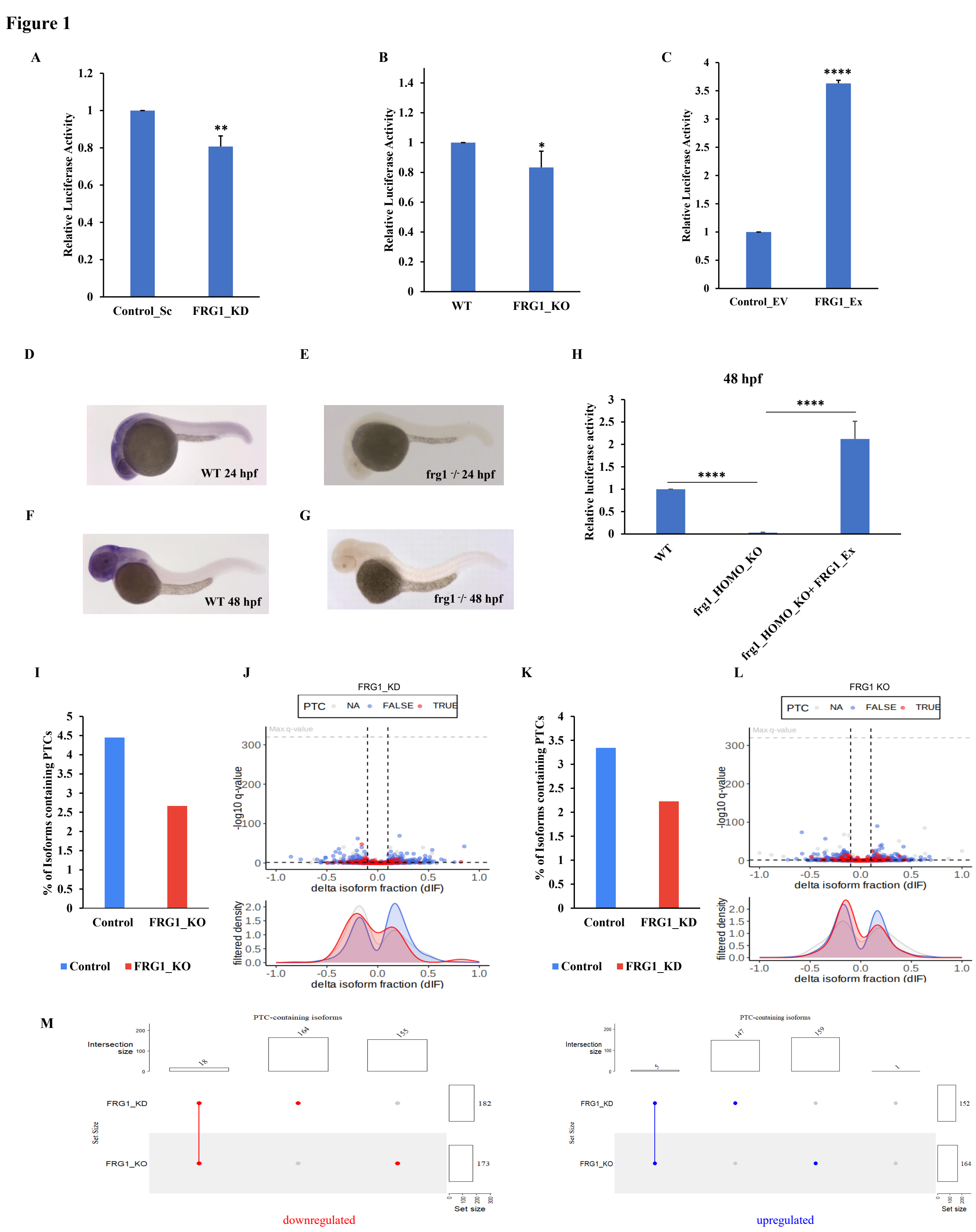
A
Relative Luciferase Activity
Control_Sc
FRG1_KD
B
Relative Luciferase Activity
WT
FRG1_KO
C
Relative Luciferase Activity
Control_EV
FRG1_Ex
D
WT 24 hpf
E
frg1 -/- 24 hpf
F
WT 48 hpf
G
frg1 -/- 48 hpf
H
48 hpf
Relative luciferase activity
WT
frg1_HOMO_KO
frg1_HOMO_KO+ FRG1_Ex
I
% of Isoforms containing PTCs
Control
FRG1_KO
J
FRG1_KD
PTC NA FALSE TRUE
Max q-value
-log10 q-value
delta isoform fraction (dIF)
filtered density
K
% of Isoforms containing PTCs
Control
FRG1_KD
L
FRG1 KO
PTC NA FALSE TRUE
Max q-value
-log10 q-value
delta isoform fraction (dIF)
filtered density
M
PTC-containing isoforms
Intersection size
FRG1_KD
FRG1_KO
Set Size
Set size
downregulated
upregulated

Figure 2

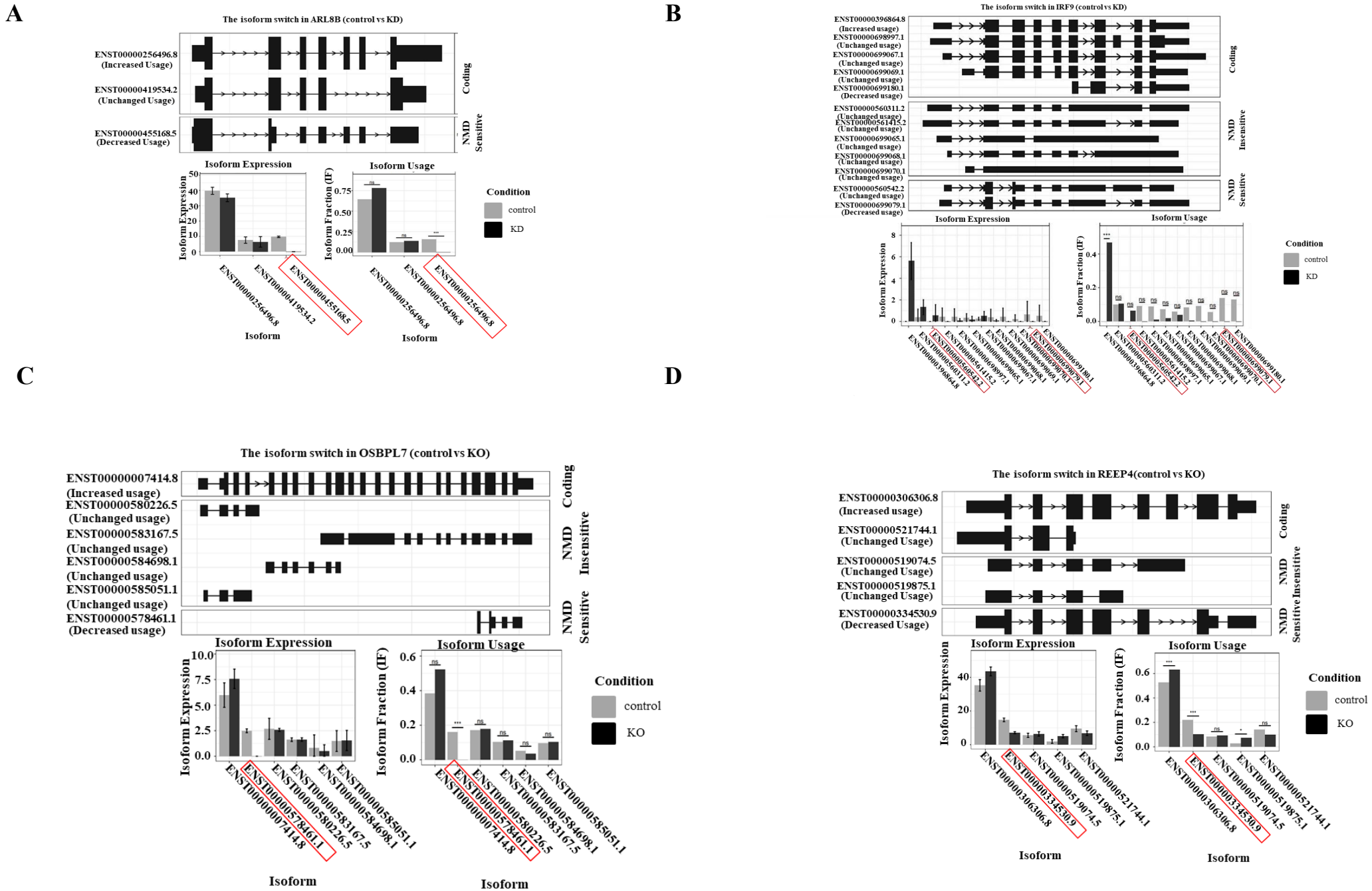
A
The isoform switch in ARL8B (control vs KD)
ENST00000256496.8 (Increased Usage)
ENST00000419534.2 (Unchanged Usage)
ENST00000455168.5 (Decreased Usage)
Coding
NMD Sensitive
Isoform Expression
Isoform Usage
Isoform Expression
Isoform Fraction (IF)
Condition
control
KD
Isoform
B
The isoform switch in IRF9 (control vs KD)
Coding
NMD Insensitive
NMD Sensitive
Isoform Expression
Isoform Usage
Condition
control
KD
C
The isoform switch in OSBPL7 (control vs KO)
ENST00000007414.8 (Increased usage)
ENST00000580226.5 (Unchanged usage)
ENST00000583167.5 (Unchanged usage)
ENST00000584698.1 (Unchanged usage)
ENST00000585051.1 (Unchanged usage)
ENST00000578461.1 (Decreased usage)
Coding
NMD Insensitive
NMD Sensitive
Isoform Expression
Isoform Usage
Isoform Expression
Isoform Fraction (IF)
Condition
control
KO
Isoform
D
The isoform switch in REEP4(control vs KO)
ENST00000306306.8 (Increased usage)
ENST00000521744.1 (Unchanged Usage)
ENST00000519074.5 (Unchanged Usage)
ENST00000519875.1 (Unchanged Usage)
ENST00000334530.9 (Decreased Usage)
Coding
NMD Insensitive
NMD Sensitive
Isoform Expression
Isoform Usage
Isoform Expression
Isoform Fraction (IF)
Condition
control
KO
Isoform

Figure 3

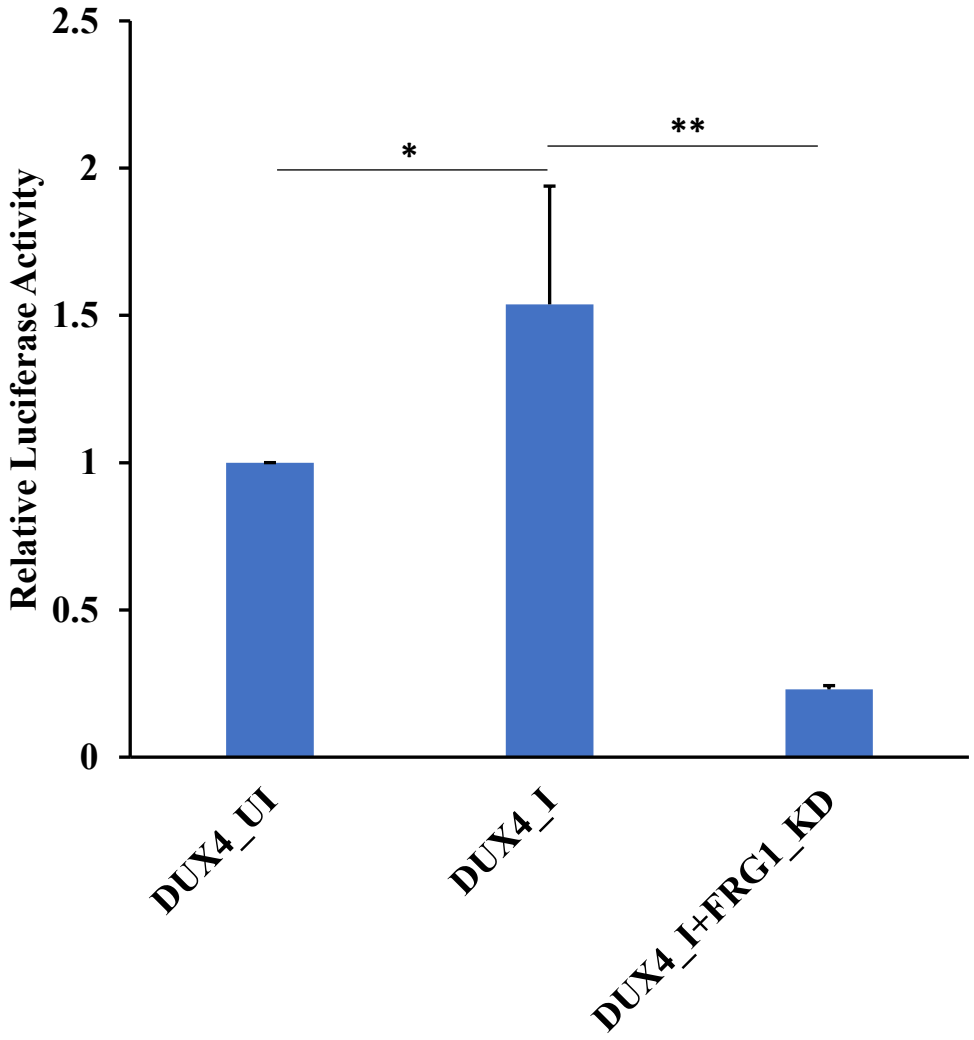
2.5
2
1.5
1
0.5
0
Relative Luciferase Activity
*
**
DUX4_UI
DUX4_I
DUX4_I+FRG1_KD

Figure 4

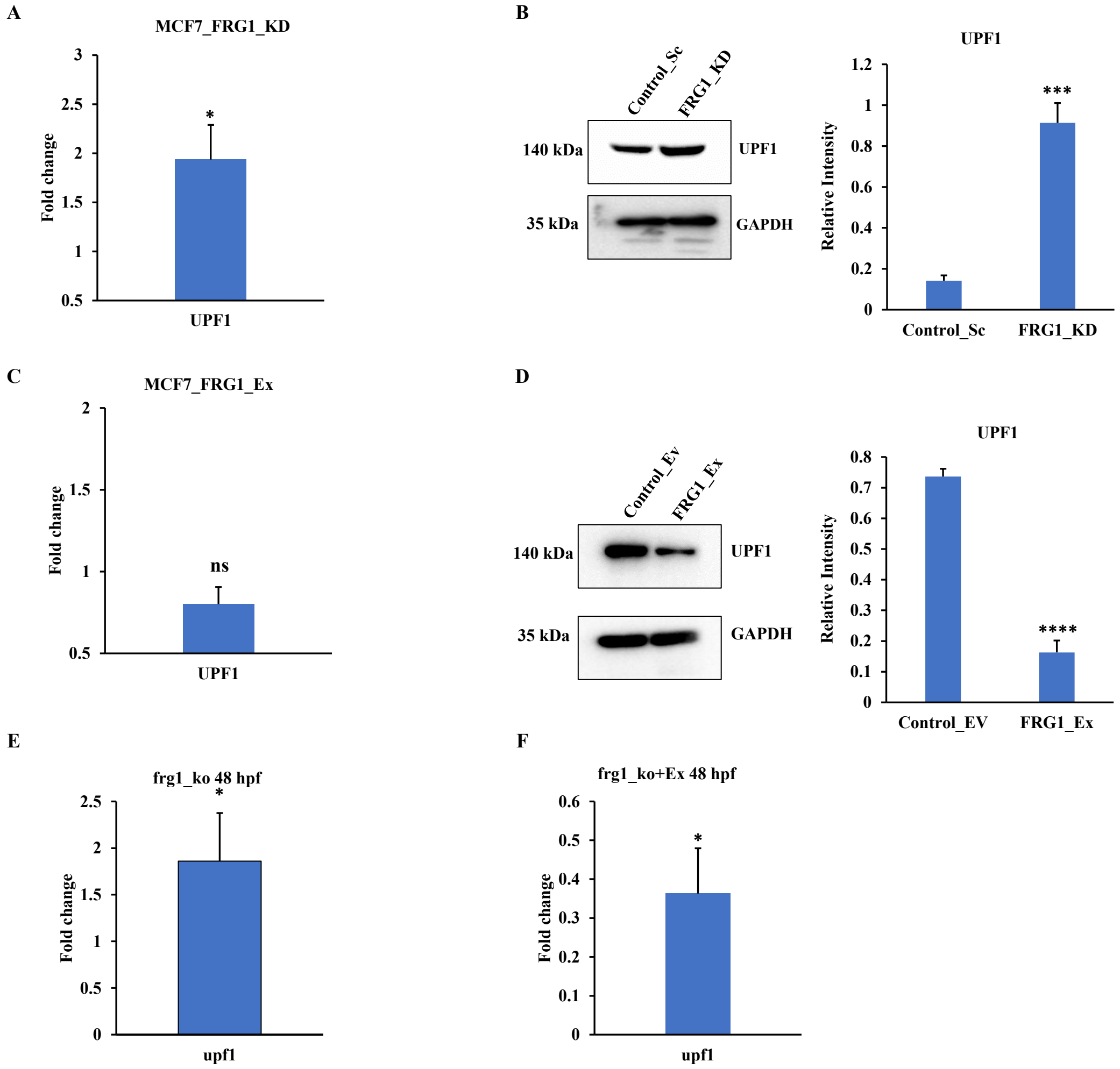
A
MCF7_FRG1_KD
Fold change
3
2.5
2
1.5
1
0.5
*
UPF1
B
Control_Sc
FRG1_KD
140 kDa
UPF1
35 kDa
GAPDH
UPF1
Relative Intensity
1.2
1
0.8
0.6
0.4
0.2
0
***
Control_Sc
FRG1_KD
C
MCF7_FRG1_Ex
Fold change
2
1.5
1
0.5
ns
UPF1
D
Control_Ev
FRG1_Ex
140 kDa
UPF1
35 kDa
GAPDH
UPF1
Relative Intensity
0.8
0.7
0.6
0.5
0.4
0.3
0.2
0.1
0
****
Control_EV
FRG1_Ex
E
frg1_ko 48 hpf
Fold change
2.5
2
1.5
1
0.5
0
*
upf1
F
frg1_ko+Ex 48 hpf
Fold change
0.6
0.5
0.4
0.3
0.2
0.1
0
*
upf1

Figure 5

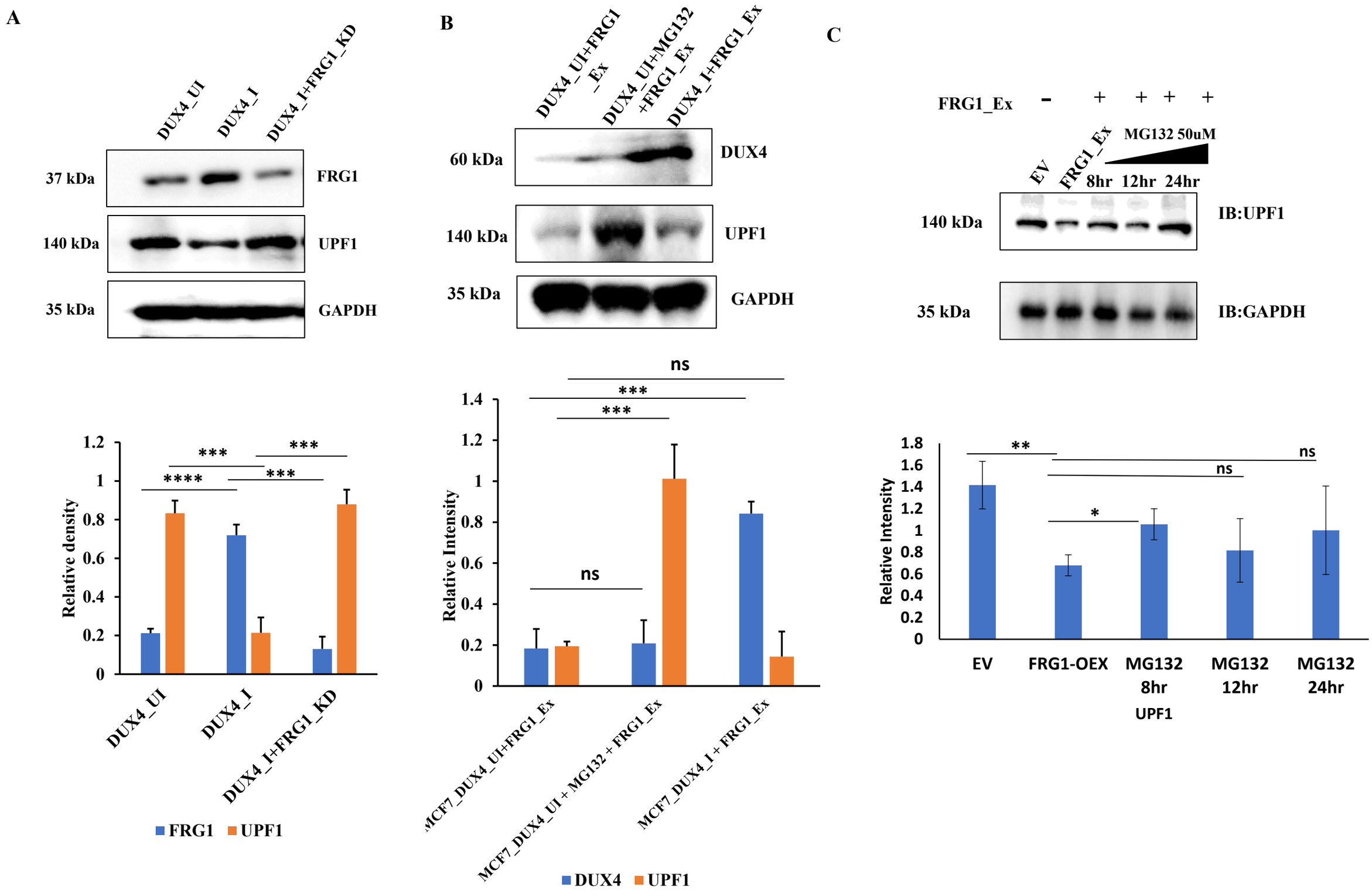
A
DUX4_UI
DUX4_I
DUX4_I+FRG1_KD
37 kDa
FRG1
140 kDa
UPF1
35 kDa
GAPDH
Relative density
1.2
1
0.8
0.6
0.4
0.2
0
****
***
***
***
DUX4_UI
DUX4_I
DUX4_I+FRG1_KD
FRG1
UPF1
B
DUX4_UI+FRG1_Ex
DUX4_UI+MG132+FRG1_Ex
DUX4_I+FRG1_Ex
60 kDa
DUX4
140 kDa
UPF1
35 kDa
GAPDH
Relative Intensity
1.4
1.2
1
0.8
0.6
0.4
0.2
0
ns
***
***
MCF7_DUX4_UI+FRG1_Ex
MCF7_DUX4_UI + MG132 + FRG1_Ex
MCF7_DUX4_I + FRG1_Ex
DUX4
UPF1
C
FRG1_Ex
-
+
+
+
+
EV
FRG1_Ex
MG132 50uM
8hr
12hr
24hr
140 kDa
IB:UPF1
35 kDa
IB:GAPDH
Relative Intensity
1.8
1.6
1.4
1.2
1
0.8
0.6
0.4
0.2
0
**
ns
ns
*
EV
FRG1-OEX
MG132 8hr
MG132 12hr
MG132 24hr
UPF1

Figure 6 New

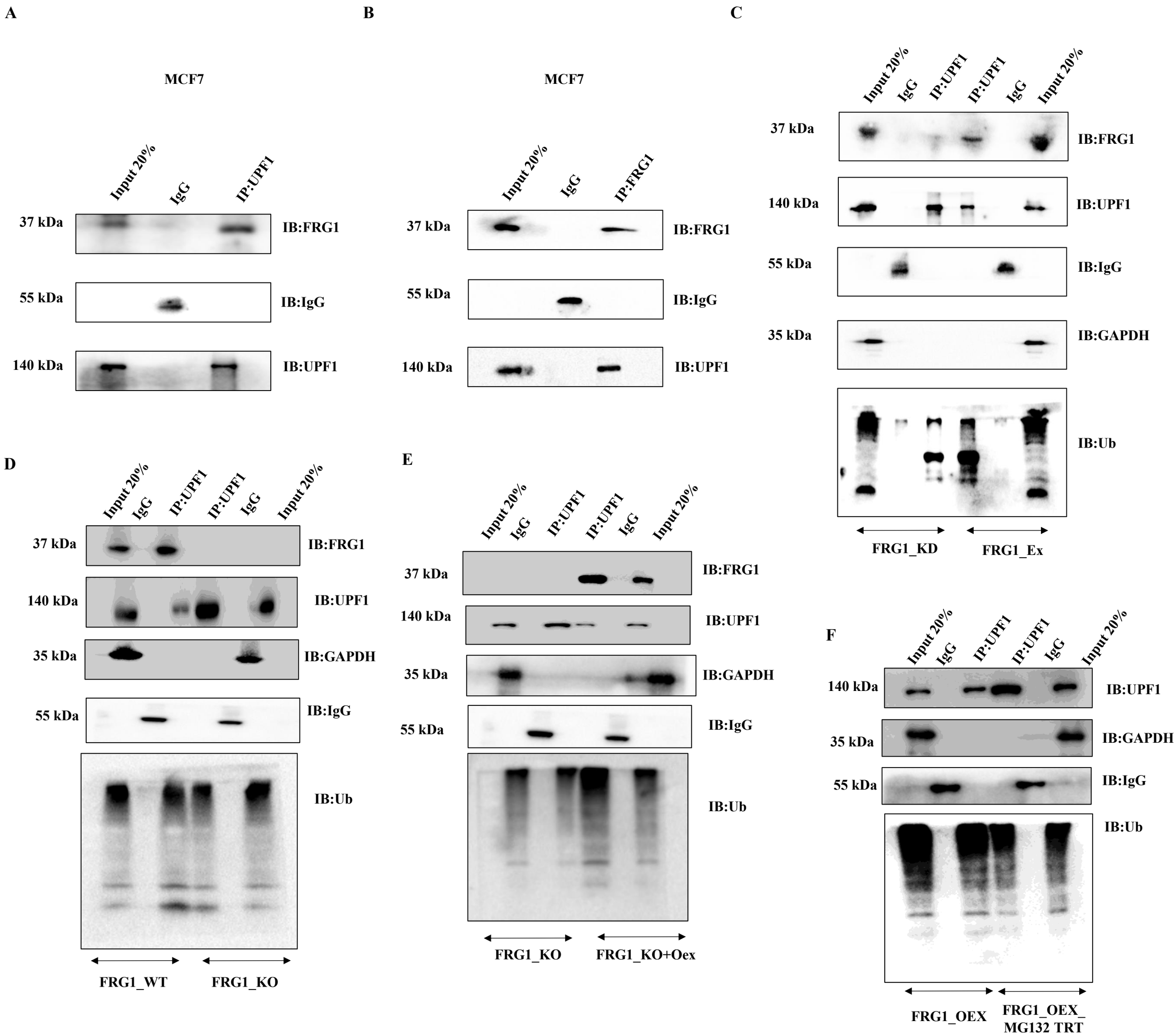
A
MCF7
Input 20%
IgG
IP:UPF1
37 kDa
IB:FRG1
55 kDa
IB:IgG
140 kDa
IB:UPF1
B
MCF7
Input 20%
IgG
IP:FRG1
37 kDa
IB:FRG1
55 kDa
IB:IgG
140 kDa
IB:UPF1
C
Input 20%
IgG
IP:UPF1
IP:UPF1
IgG
Input 20%
37 kDa
IB:FRG1
140 kDa
IB:UPF1
55 kDa
IB:IgG
35 kDa
IB:GAPDH
IB:Ub
FRG1_KD
FRG1_Ex
D
Input 20%
IgG
IP:UPF1
IP:UPF1
IgG
Input 20%
37 kDa
IB:FRG1
140 kDa
IB:UPF1
35 kDa
IB:GAPDH
55 kDa
IB:IgG
IB:Ub
FRG1_WT
FRG1_KO
E
Input 20%
IgG
IP:UPF1
IP:UPF1
IgG
Input 20%
37 kDa
IB:FRG1
140 kDa
IB:UPF1
35 kDa
IB:GAPDH
55 kDa
IB:IgG
IB:Ub
FRG1_KO
FRG1_KO+Oex
F
Input 20%
IgG
IP:UPF1
IP:UPF1
IgG
Input 20%
140 kDa
IB:UPF1
35 kDa
IB:GAPDH
55 kDa
IB:IgG
IB:Ub
FRG1_OEX
FRG1_OEX_
MG132 TRT

Figure 7

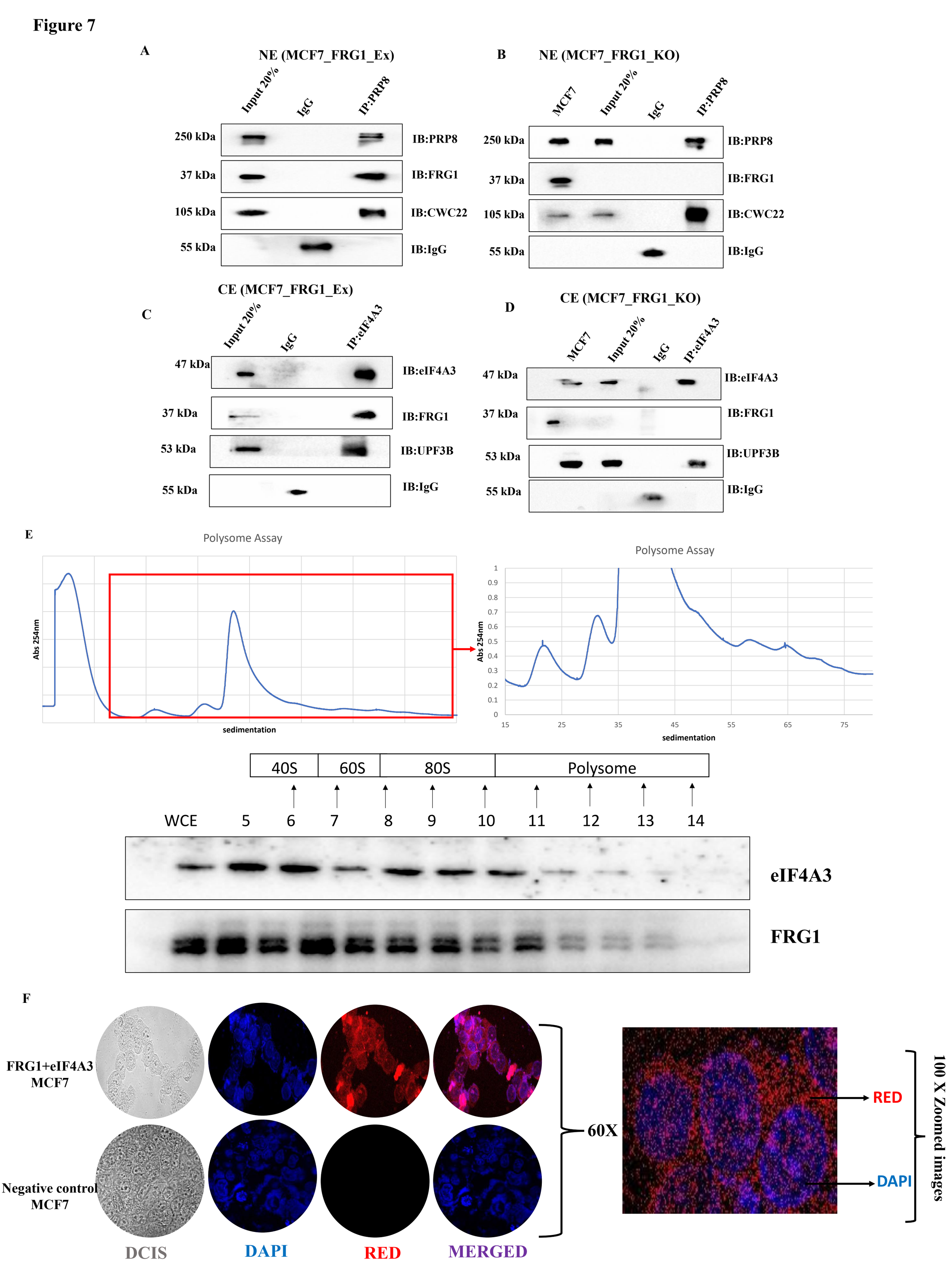
A
NE (MCF7_FRG1_Ex)
Input 20%
IgG
IP:PRP8
250 kDa
IB:PRP8
37 kDa
IB:FRG1
105 kDa
IB:CWC22
55 kDa
IB:IgG
B
NE (MCF7_FRG1_KO)
MCF7
Input 20%
IgG
IP:PRP8
250 kDa
IB:PRP8
37 kDa
IB:FRG1
105 kDa
IB:CWC22
55 kDa
IB:IgG
C
CE (MCF7_FRG1_Ex)
Input 20%
IgG
IP:eIF4A3
47 kDa
IB:eIF4A3
37 kDa
IB:FRG1
53 kDa
IB:UPF3B
55 kDa
IB:IgG
D
CE (MCF7_FRG1_KO)
MCF7
Input 20%
IgG
IP:eIF4A3
47 kDa
IB:eIF4A3
37 kDa
IB:FRG1
53 kDa
IB:UPF3B
55 kDa
IB:IgG
E
Polysome Assay
Abs 254nm
sedimentation
Polysome Assay
Abs 254nm
sedimentation
40S
60S
80S
Polysome
WCE
5
6
7
8
9
10
11
12
13
14
eIF4A3
FRG1
F
FRG1+eIF4A3
MCF7
Negative control
MCF7
DCIS
DAPI
RED
MERGED
60X
RED
DAPI
100 X Zoomed images
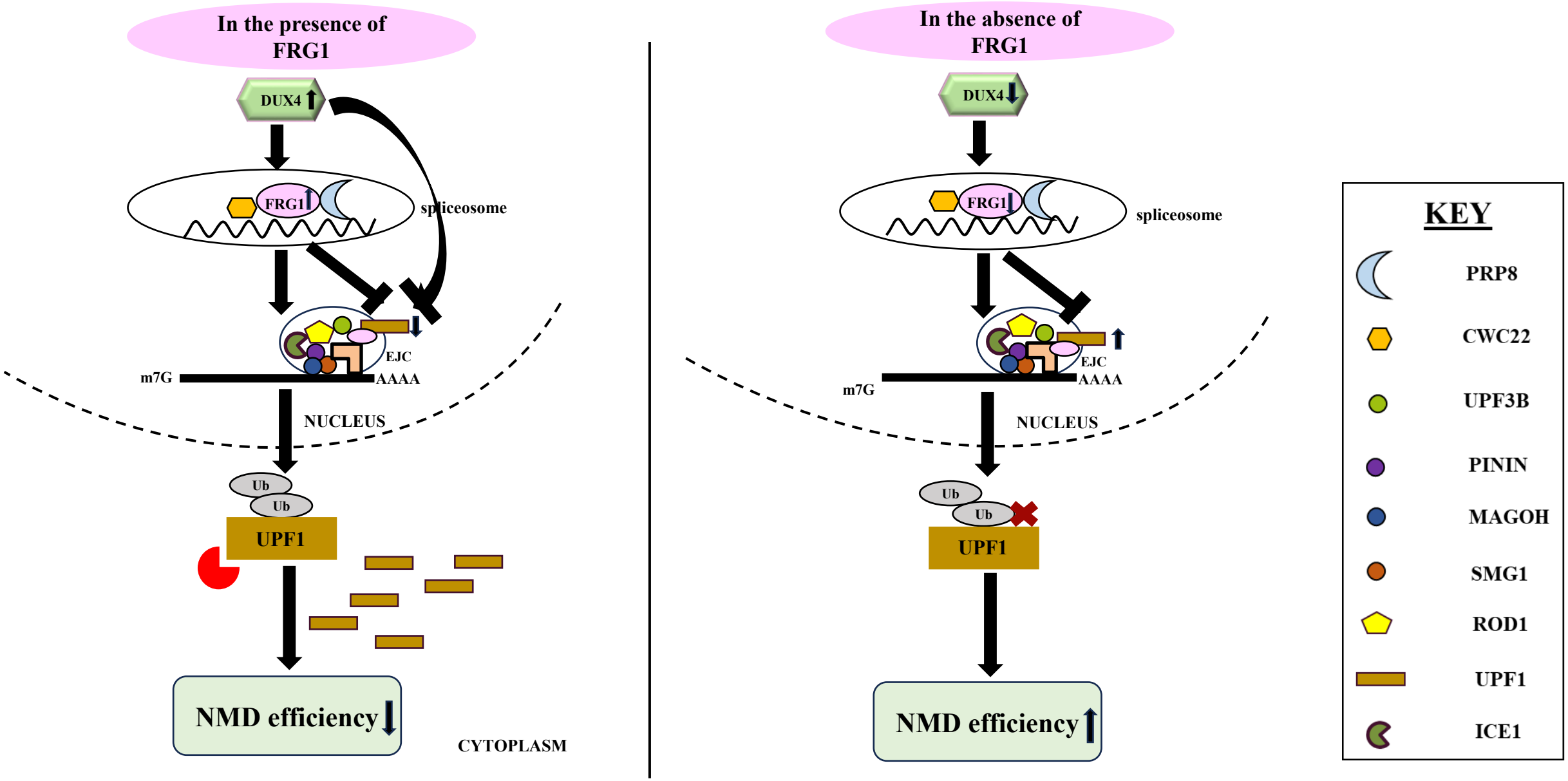
Graphical Abstract